CHAPTER 12

ELECTRICAL EXPLORATION METHODS FOR THE SEAFLOOR

Alan D. Chave, Steven C. Constable,‡ and R. Nigel Edwards§*

INTRODUCTION

Recent developments in instrumentation and submarine geology have spawned increasing interest in the use of electromagnetic (EM) methods for seafloor exploration. Previously, little attention had been given to their use in the marine environment, due both to the success of the seismic techniques in delineating subsurface structure and to a pervasive belief that the high electrical conductivity of seawater precluded the application of EM principles. Marine EM exploration of the solid earth has progressed substantially in academic circles over the past two decades; the adaptation of this technology for commercial purposes is only beginning.

Over three-fifths of the earth's surface is covered by oceans. Even though petroleum is produced from huge deposits on the relatively shallow continental shelf, the immense area of the ocean represents a largely unexplored and unexploited resource base. Until recently, little economic interest was shown in the ocean floor environment; with the possible exception of manganese nodule fields (Sorem and Fewkes, 1979) and the heavy metal-rich brines found in intracratonic basins like the Red Sea (Degens and Ross, 1969), the seafloor was assumed to be essentially barren. However, the recent discovery of intense hydrothermal activity and polymetallic sulfide deposits of unprecedented concentration and scale on the crest of the East Pacific Rise (Hekinian et al., 1983; Spiess et al., 1980; Ballard et al., 1981), the Galapagos Ridge (Corliss et al., 1979), the Juan de Fuca Ridge (Normark et al., 1983; Koski et al., 1985), and the Mid-Atlantic Ridge (Rona et al., 1986) has aroused interest in the possibility of deep-sea mining and spurred research into mid-ocean ridge ore genesis as an analog to terrestrial occurrences; see Teleki et al. (1985), Brimhall (1987), and Rona (1987) for comprehensive reviews of these topics. The sulfide deposits were located visually with submersibles or using near-bottom survey tools such as ANGUS (Phillips et al., 1979). While these methods are capable of examining surficial geology, they are not able to adequately assess the actual extent of the deposits and the nature of the geological structures in which they are found. Seafloor conductivity mapping is one of the few geophysical tools suitable for this purpose, just as the EM methods are one of the major geophysical techniques used in mineral exploration on land.

Over the past few decades, the search for petroleum reserves has been extended from the continents offshore into progressively deeper water, making the continental shelves a focus for geophysical exploration. The principal geophysical tool for this is the seismic method, and the success of the seismic approach is attested to by the level of offshore drilling activity and the subsequent production of oil. However, there are marine geological terranes in which the interpretation of seismic data is difficult, such as regions dominated by scattering or the high reflectivity that is characteristic of carbonate reefs, volcanic cover, and submarine permafrost. Alternative, complementary geophysical techniques are required to study these regions.

In recent years, significant advances have been recorded in theory, methodology, and instrumentation for the marine EM methods. Many of the seafloor techniques are adaptations of standard terrestrial EM approaches, while others represent new directions.

*AT&T Bell Laboratories, Murray Hill, NJ 07974, and Scripps Institution of Oceanography, La Jolla, CA 92093.
‡Scripps Institution of Oceanography, La Jolla, CA 92093.
§Department of Physics, University of Toronto, Toronto, Ontario M5S 1A7 CANADA.

This paper emphasizes the differences between seafloor and terrestrial EM applications, especially with regard to noise, resolving ability, and apparatus. The ocean environment and its impact on EM measurements and equipment is discussed in some detail, and then the specific practice of magnetotelluric, dc resistivity, magnetometric resistivity, self potential, and frequency- and time-domain controlled source EM sounding is described. A comprehensive review of pertinent literature is included. Most of the existing work on seafloor EM has been motivated by solid earth problems, as opposed to exploration ones. The real data discussed reflect this difference, which is principally one of scale.

THEORY

There are numerous approaches to the theory of EM induction in conducting media by finite or distant sources; see Ward and Hohmann, Vol. 1 (1988) for a review. From the point of view of both computational ease and preservation of essential physics, the modal form of the induction equations for one-dimensional (1-D) media is especially appealing and has been adopted here. The EM fields for a 1-D conductivity structure may be separated into independent toroidal and poloidal magnetic (TM and PM) modes about the vertical axis. The TM modes are associated with electric currents flowing in loops containing the vertical, and possess no vertical magnetic field component, while PM modes are driven by electric current systems which are always horizontal, and have no vertical electric field component. Because of this distinction, the sensitivity of the two modes to electrical structure is quite different. This difference can be demonstrated most vividly by imagining a horizontal insulating layer buried in a half-space, and deducing the behavior of vertical and horizontal currents in its presence. Due to the existence of vertical electric currents and consequent galvanic interactions, TM modes are strongly affected by relatively low conductivity zones, being unable to penetrate them very effectively, while the PM mode is quite insensitive to such regions due to its entirely inductive nature. Both modes are influenced by relatively high conductivity material. A summary of mode theory appears in the appendix, including Green functions which account for seafloor and sea-surface boundary effects explicitly, and will be referred to as needed.

THE OCEANIC ENVIRONMENT

The continents are in direct contact with a near insulator, the atmosphere, which allows the nearly instantaneous propagation of EM signals with limited attenuation. To the electrical prospector, the seafloor is a very different environment. The seafloor is covered by up to 11 km of seawater that has conductivity ranging in value from as much as 5 S/m near the surface to about 3.2 S/m below the main thermocline; the latter typically occurs at depths of a few hundred meters in the deep ocean. The conductivity of seawater is controlled almost entirely by temperature and salinity, with a negligible pressure effect (Horne and Frysinger, 1963). To a reasonable approximation, the conductivity of seawater is given by

$$\sigma(T) = 3 + T/10 \qquad (1)$$

where σ is the conductivity in S/m and T is the in situ temperature in degrees centigrade. This conductivity value is higher than that of most of the materials which lie at or below the seafloor. The uppermost sediments under the ocean are usually water-saturated, and have conductivities of 0.1–1.0 S/m. On the continental shelves, this value decreases as lithification and diagenesis reduce the porosity of the sediments, until the deep structure of the shelves is much like that of the rest of the continents. By contrast, sediments in the deep ocean are rarely thicker than a few hundred meters, and are underlain by a basaltic crust and peridotitic mantle whose conductivity decreases from about 0.1 S/m near the top to values that may be more than 1000 times smaller at depths of 10 km or less.

The highly conductive ocean acts as a low pass filter for fluctuating EM fields generated above it in the ionosphere and magnetosphere. Little power is present at the seafloor at frequencies above a fraction of a hertz in water greater than a few hundred meters deep from these types of sources. Contamination by man-made or cultural sources is substantially reduced by the seawater layer, and need not be considered in most deep-ocean experiments. However, this may be an important noise source on the continental shelf close to cities, where signals could propagate offshore through low conductivity seafloor layers. The ocean filtering effect may be quantified by the use of a simple model. Consider a seawater layer of thickness H and conductivity σ_0 overlying a 1-D earth and underlying an insulating atmosphere. A vertical magnetic dipole-like source of intrinsic frequency ω a large distance above the water produces normally incident magnetic fields at the sea surface; this range is assumed sufficient that the source produces only plane waves. Chave and Filloux (1984) give expressions from which the ratio of seafloor-to-sea surface horizontal electric (E_{sf}/E_{ss}) and magnetic (B_{sf}/B_{ss}) fields may be computed

$$\frac{E_{sf}}{E_{ss}} = \frac{(1 + R_L^{\mathrm{PM}})e^{-\gamma_0 H}}{1 + R_L^{\mathrm{PM}} e^{-2\gamma_0 H}}, \qquad (2)$$

and

$$\frac{B_{sf}}{B_{ss}} = \frac{(1 - R_L^{PM})e^{-\gamma_0 H}}{1 - R_L^{PM} e^{-2\gamma_0 H}}, \tag{3}$$

where R_L^{PM} is the PM mode seafloor reflection coefficient (see A-16 in the appendix), and

$$\gamma_0 = \sqrt{i\omega\mu_0\sigma_0} \tag{4}$$

is the induction parameter or the reciprocal of the complex skin depth. Due to the large conductivity contrast between seawater and crustal rock and the assumption of zero source field wavenumber, the magnitude of the reflection coefficient is close to unity. Equations (2) and (3) reduce to simple exponential field attenuation at a depth H in an infinitely deep ocean when $R_L^{PM} = 0$. Figure 1 shows the two expressions (2) and (3) evaluated for ocean depths of 5000, 500, and 100 m, covering the range from the deep ocean to the continental shelf, and for earth halfspaces of conductivity 0.005 and 0.05 S/m. The horizontal electric field ratio is insensitive to the conductivity beneath the observation site and displays marked attenuation only when the water layer becomes electrically thick ($\gamma_0 H \gg 1$). By contrast, the horizontal magnetic field ratio is quite sensitive to earth conductivity and is attenuated more than the electric field even at very long periods. The vertical magnetic field behaves like the horizontal electric field, and is attenuated only at relatively short periods. The natural, ionospheric and magnetospheric, electromagnetic spectrum is highly nonstationary, varying over several decades from day-to-day in all parts of the spectrum, and displays a strong dependence on location, increasing at high latitudes and around certain geologic anomalies. For this reason, there is no "typical" EM source spectrum from which a seafloor model may be deduced by applying the filters given as equations (2)–(3). However, in the deep ocean, the attenuation of magnetic fields at periods smaller than 100 s is very large, exceeding 10^6 in power, and virtually no EM energy reaches the seafloor below this period. In shallow water, such severe magnetic field reduction occurs at periods of around 1 s. By contrast, the attenuation of the electric field is only a factor of 100 at around 10 s period in the deep ocean, and is not observable at periods longer than 1 s in shallow water.

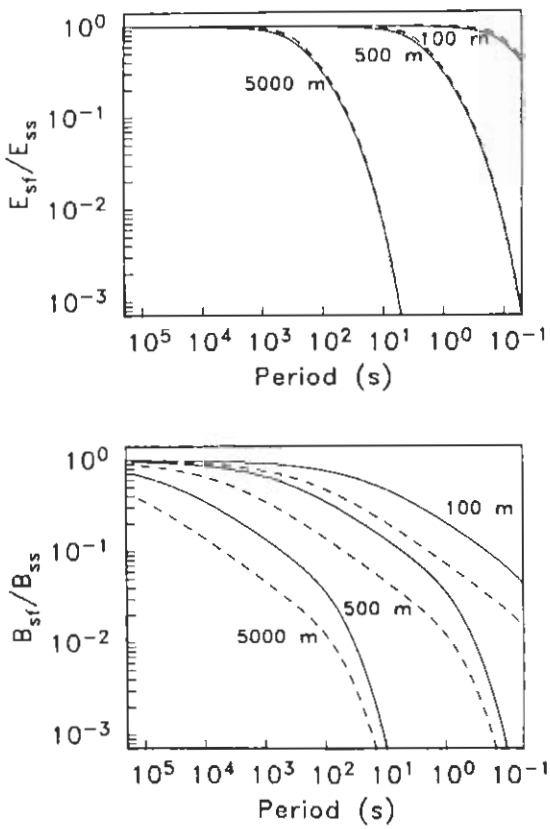

Fig. 1. The ratios of the seafloor-to-sea surface horizontal electric (top) and horizontal magnetic (bottom) fields as a function of period in the zero source field wavenumber limit. The earth is modeled as an insulating atmosphere overlying an ocean layer of conductivity 3.2 S/m and thickness 5000, 500, and 100 m and underlain by a halfspace of conductivity 0.05 S/m (solid lines) or 0.005 S/m (dashed lines). Attenuation of the vertical magnetic field is similar to that of the horizontal electric field.

The ocean is in continual motion on all spatial and temporal scales, generating EM fields by dynamo interaction with the earth's magnetic field in a manner identical to the principle of an electric generator. EM field generation by water motion is a complex subject. Since the Maxwell equations constitute a linear set, the fields occur on space and time scales similar to those of the variability of the ocean, covering periods from years to seconds and wavelengths from thousands of kilometers to centimeters. However, the large spatial scales generally correlate with the long period disturbances, and problems with oceanic EM fields as a noise source are completely different for long period magnetotellurics (MT) and high frequency controlled source EM.

Long period (>1 h) EM fields in the deep ocean are discussed in Cox et al. (1971), Cox (1980, 1981), Chave and Filloux (1984), Chave (1984a), Chave and Filloux (1985), Lilley et al. (1986), and Chave et al. (1989), while a major physical oceanographic experiment based on their measurement is described in Luther et al. (1987, 1990). At periods longer than three to five days, mesoscale eddy activity and a background barotropic (depth-independent) water velocity component produce intense electric fields, reducing the coherence between seafloor electric and magnetic measurements substantially. This is particularly pro-

nounced in the westward portion of ocean basins because mesoscale eddies are continually being shed by the intense currents (e.g., the Gulf Stream) that dominate the dynamics of those regions. In addition, the ocean tides produce sizable electric and magnetic fields (Larsen, 1968). Because of the strong motional contribution to the EM field, it is not possible to utilize external source sounding methods at periods longer than a few days. It is also probable that the ubiquitous oceanic internal waves produce a magnetic signature that affects seafloor measurements at periods of 1–4 h, depending on the level of geomagnetic activity and the latitude.

Additional complications appear on the continental shelves: the water velocity field is substantially more energetic and complex than at the deep ocean floor, and possible topographic effects from rugged shelf topography may appear at high frequencies. The dynamics of the circulation on the continental shelves is not well understood, but new classes of waves that are trapped to the topography are possible on many spatial and temporal scales, and interactions of warm currents with topography can generate new, small-scale water currents whose EM effects will be important at the seafloor. The generally higher velocities will combine with rough shelf topography to produce local turbulence. The EM fields generated by oceanic turbulence are discussed in Cox et al. (1971); the electric fields associated with turbulence may be locally intense, while the magnetic signature is negligible.

At higher frequencies, surface gravity waves, microseisms, swell, and wind waves produce velocity and pressure fluctuations at the seafloor that in turn induce local EM fields. At periods longer than 40 s, direct forcing by surface gravity waves produces a rapidly rising noise spectrum toward longer periods even in the deep ocean. Measurements indicate that the fluctuating ionospheric component in seafloor electric field measurements often dominates the gravity wave part, but the latter serves as a relatively stationary base below which the spectrum cannot decrease, determining the ultimate noise level (Webb and Cox, 1986). At periods of 10–40 s, the spectrum of electric field variations on the seafloor decreases as the wavelength of the gravity modes becomes smaller, but a background noise component in the electric field of indeterminate origin remains (Webb and Cox, 1986).

Cox et al. (1978) conducted a thorough experimental and theoretical study of the EM fields produced by microseisms, which are caused by the nonlinear interference of opposing surface gravity wave trains. This produces a pressure disturbance at twice the intrinsic frequency of the waves which propagates to the seafloor even in deep water, resulting in horizontal water motions which generate ambient EM fields. As a consequence, sharply peaked EM spectra having an amplitude one to three decades above the background and centered on 0.1–0.3 Hz are observed; multiple peaks can occur due to the presence of swell from distant storms combined with local wind forcing and reflections from nearby coastlines. Webb and Cox (1986) presented measurements of the seafloor electric field due to microseisms, and the evolution of its spectrum during a storm. Webb and Cox (1982, 1986) have also investigated the EM effects of seafloor acoustic and seismic disturbances. They describe the effect of resonances of seismic surface waves that results in acoustic energy being trapped near the seafloor and multiple peaks in the EM spectrum. The background noise between these narrow-band features in the electric field spectra is probably due to small-scale (0.1 m) turbulent eddies (Cox et al., 1978). Figure 2 illustrates all of these high frequency phenomena. It should be emphasized that the background oceanic noise at high frequencies is complex and not completely understood, with a strong dependence on sea state and local geology.

The effect of these two main noise sources—external and oceanic—is different for the passive and active EM methods. Seafloor MT suffers from a band-limited source, being caught between attenuated external source fields at high frequencies and contamination by oceanic noise at long periods. The dc, self potential (SP), and controlled source methods are not influenced by long period oceanic phenomena and (except in shallow water) by ionospheric noise, but may be affected by the higher frequency sources discussed.

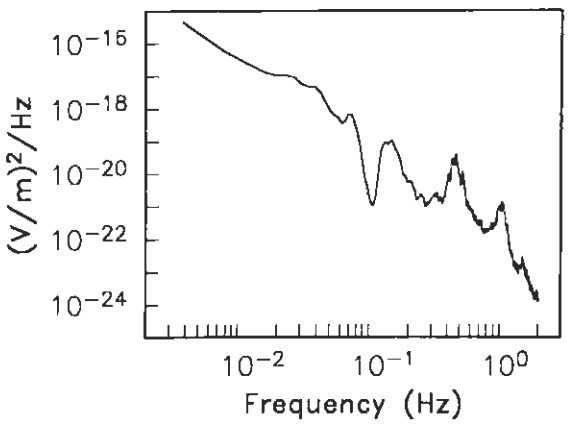

Fig. 2. Electric field power spectrum computed from measurements taken 200 km southwest of San Diego in 3700 m of water. The $\propto f^{-4}$ slope at low frequencies is caused by ionospheric activity and forcing by long surface gravity waves. The peak near 0.1 Hz is due to microseism activity at the seafloor, while the higher frequency peaks are due to Rayleigh wave-induced motion of the seafloor antenna. See text for details.

For all but one oceanic EM method (SP), the electric or magnetic fields which constitute the signal are much reduced over the values which would be encountered on land. The conductive water layer which is responsible for this decrease in amplitude produces some compensatory benefits; the measurement of these smaller signals is possible if correct advantage is taken of the marine environment. Potential electrode noise is reduced throughout the spectrum because low impedance contact with seawater is easily established, and the ocean provides thermal and saline stability at a level never observed on land. Transmitter electrodes are also less of a problem than on land, where considerable labor is often required to obtain resistances to ground of 10 Ω. At sea, a grounding resistance of 0.1 Ω can be obtained merely by lowering a long, uninsulated cable or pipe into the water.

Only magnetic sources and receivers can be towed over land, but these must be well off the ground for safety reasons and are usually attached to an aircraft. By contrast, in the ocean both transmitter and receiver electrodes may be towed through the water and close to the seabed. Near-bottom towing introduces new sources of noise caused by antenna cables moving in the earth's magnetic field and streaming potentials or turbulent flows that affect potential electrodes, but these problems are outweighed by the greatly increased areal coverage that can be achieved. This makes new types of survey tools possible in the ocean that have no counterpart on land.

Another advantage offered by the conductive ocean is its smoothing effect on electric fields. Except for regions of extreme bottom relief (e.g., mid-ocean ridges and the continental slope), the uniformity and great electrical thickness of the water column, combined with the large conductivity of seawater, will dominate the effect of small-scale irregularities in the near-bottom rocks, yielding electric field measurements that are homogeneous over large areas. This is quite apparent in Atlantic array data at periods of several days, where very good coherence between electric field stations separated by over 100 km was observed (Cox et al., 1980; Cox, 1980), and should be contrasted with the usual situation on land, where near-surface heterogeneity degrades the electric field coherence substantially, even when the distance between measurements is quite small.

Operating at sea does create special technical difficulties associated with maintaining equipment in a hostile environment. Most of the packaging techniques used are common to all of the methods described later. Seafloor equipment must be housed in watertight vessels capable of withstanding 100–1000 atmospheres of hydrostatic pressure. Made out of aluminum or glass, these vessels are usually spherical or cylindrical for mechanical strength and volumetric efficiency. Although it is possible to connect floating surface packages to seafloor equipment, such moorings are very costly and time consuming to deploy and recover. Instead, most receiving instruments are self-contained, operating off battery power and collecting data under the control of a small computer. Measurements are usually stored on magnetic tape, although solid state memory is beginning to supplant tape. A means to orient the measurements with respect to the earth after instrument emplacement is sometimes necessary; photographic recording of a compass is commonly used. The packages are buoyant to facilitate recovery, and attachment of a heavy anchor allows them to be lowered or dropped in free fall to the ocean bottom. When necessary, instruments may be located at the seafloor using standard acoustic ranging techniques. After data collection a timed or acoustically triggered release causes the instrument to part from the anchor and float to the surface, where it is recovered with the aid of radio and strobe light beacons.

Seafloor electric field receivers, as with terrestrial types, consist of a pair of electrodes connected to a recording voltmeter. The standard oceanic electrode is of silver-silver chloride (Ag-AgCl) type, and their construction is discussed in Filloux (1973, 1974, 1987) and in Webb et al. (1985). A great deal of progress in electrode noise reduction has been made in recent years, but this factor looms large in limiting the sensitivity of oceanic electric field measurements. The principal noise sources include electrochemical effects associated either with contamination during construction or with natural processes in the ocean, temperature and salinity fluctuations associated with small-scale turbulence, and streaming potentials or other electrokinetic phenomena. Most of these effects are not well understood, and a largely empirical approach to their reduction has been employed. The ultimate limitation is due to the Johnson noise associated with the electrode, antenna, and input impedance of the amplifiers; this noise is about $10^{-19} V^2/Hz$ for the Webb et al. (1985) high frequency electrodes.

MAGNETOTELLURICS

The magnetotelluric (MT) method is a standard way of determining the electrical conductivity distribution beneath and around a measuring point using the natural electric and magnetic fields induced in the earth by ionospheric and magnetospheric electric current systems. The theory and principles behind MT are covered both in Vozoff (1972, and this volume) and in Kaufman and Keller (1981), and are not changed appreciably for marine applications. However, oceanic MT measurements must be made on the seafloor

because magnetometer motion has to be eliminated; this arrangement precludes operation from either subsurface moorings or surface ships.

The two major physical phenomena which differentiate marine from terrestrial MT techniques are the high-frequency cutoff of the source spectrum at the seafloor caused by induction in the conducting ocean and the generation of EM fields by water motion. This differentiation results in a seafloor EM spectrum for solid earth MT purposes that is band-limited in the deep ocean, being cut off at both high and low frequencies by different phenomena. While the amplitude reduction of the seafloor fields is an important constraint in instrumental and experimental design, the seafloor MT response function or impedance does not depend on the thickness of the water layer and is a measure only of the suboceanic conductivity structure. However, the application of MT methods in the deep ocean is generally limited to periods longer than a few minutes, and the audiomagnetotelluric (AMT) method cannot be used even on the continental shelf. The extent and importance of contamination of existing, low-frequency MT data by motional fields is not well-understood, and its potential as a problem at the higher frequencies of interest in exploration geophysics is not well appreciated. It should be noted that motional sources produce EM fields that are both mixed mode and short spatial wavelength in nature, so that they do not serve as a good geophysical source, and their influence on MT measurements and their subsequent interpretation could be profound. Turbulent flow associated with continental shelf topography could be a serious noise problem for shallow water MT work, primarily through contamination of the electric field. While many of these complications can be minimized by avoiding regions of extreme bottom relief, a better understanding of these phenomena awaits the actual collection of measurements on the continental shelves.

Another problem in oceanic MT is associated with the large electrical contrast between the oceans and continents and the probable existence of highly resistive material in the upper oceanic lithosphere. A model for the polarization of the flow of electric current induced by external sources at the ocean-continent boundary, which is the oceanic counterpart of the well-known coast effect, was presented in Cox (1980), Ranganayaki and Madden (1980), and Chave and Cox (1983). This model may introduce anisotropy into the MT response function. The component of electric current in the ocean flowing normal to the coastline must either enter the resistive continent or be deflected downward into the oceanic crust and mantle by boundary electric charges. The width of the zone over which the latter effect will be important is given by

$$L = \sqrt{P_l \Sigma_0} \tag{5}$$

where Σ_0 is the integrated ocean conductivity and P_ℓ is the integrated resistivity of the basement to some depth where it drops abruptly (typically, 30–50 km). Values for L range from 200–2000 km for basement conductivities of 10^{-2} to 10^{-6} S/m, and the influence of this boundary layer is independent of frequency. However, the evidence from MT data requires a boundary layer only a few hundred kilometers in width at most. When considered together with the controlled source results of Cox et al. (1986), which indicate a very resistive uppermost mantle for moderate age lithosphere away from the continental margin, this boundary layer suggests marked lateral heterogeneity of basement conductivity. It is probable that conductive pathways from the ocean to the deep earth exist throughout the ocean basins, most likely where the oceanic lithosphere is quite young and hot or in fluid-saturated zones at the continental margins. While the polarization effect is not a serious problem in the deep ocean, it will profoundly influence MT measurements near coastlines and on the continental shelves. This influence means that interpretation of seafloor MT data near the continents requires at least a two-dimensional (2-D) model regardless of the nature of the geological structure of interest.

The instrumentation used for seafloor MT studies is discussed in Cox et al. (1971) and Filloux (1973, 1974, 1980a). A comprehensive review of all aspects of oceanic EM apparatus is given in Filloux (1987). In general, seafloor electric and magnetic field recording is done with separate instruments. Seafloor magnetometers are an adaptation of their terrestrial counterparts to the deep ocean environment, while oceanic electric field sensors present some unique challenges. Seafloor MT apparatus is usually self-contained, with no direct connection to the sea surface. Because of the very good temperature stability at the seafloor, where variations of only a few millidegrees are expected, good thermal sensitivity characteristics are usually not a critical factor during design. However, magnetometer motion is a real problem, as the benthic boundary layer is a region of intense and variable activity (Armi and D'Asaro, 1980), suggesting the use of compact packages which present only a limited surface area to the ambient currents. By contrast, induction effects on electric field instrumentation caused by motion of the receiving antenna are negligible for the frequencies used in seafloor MT sounding.

Two types of magnetic sensors are in current use for seafloor MT experiments—the suspension units developed by Filloux and reported in Filloux (1967, 1980a, 1987) and the fluxgate units with usage reported in White (1979), Law and Greenhouse (1981), and Seg-

awa et al. (1982, 1983). Filloux's instrumentation is based on magnets suspended from torsion fibers of special design and placed in a feedback coil. Optical detectors sense the angular position of the magnet, and the current in the coil is adjusted to null the magnet position, serving as a measure of the field variations. This design has the dual advantages of having no natural noise contributions except for plastic flow or creep of the torsion fiber, which can be controlled during manufacture, and making minimal demands on the stability of the associated electronics and power supplies. The main disadvantage is the custom nature of the sensors, which are not commercially available. The suspension magnetometers are housed in self-buoyant cylindrical pressure cases, sit 1 m off of the seafloor on tripod anchors, and are capable of digital recording of the magnetic variations with a least count of 0.1–0.2 nT at a rate of 32 times per hour for six months.

Fluxgate sensors have the advantage of commercial availability and the disadvantages of requiring relatively large amounts of power and placing fairly stringent stability constraints on the associated electronics. Both Law (pers. comm., 1985) and White (1979) have adapted commercial fluxgate sensors to the seafloor, while Segawa et al. (1983) used the newer ringcores which are now appearing on the market. These units have a least-count sensitivity of 0.5–1.0 nT and display long term drift, but fluxgate technology is changing quite rapidly and these limitations are expected to diminish with time.

Two types of electric field instrumentation have been used for seafloor MT work—(1) long wire units and (2) a short arm, salt bridge apparatus utilizing chopping techniques to reduce noise. The former is simply a long (typically, 500–1000 m) insulated wire with Ag-AgCl electrodes attached at the ends and connected to a recording package. The extended antenna is used to raise the signal level well above the electrode noise level, and has the additional advantage of averaging out the electric fields generated by turbulence and temperature-salinity variations, which usually occur with a spatial scale of a few meters. The main disadvantage is the difficulty of deployment, which requires a ship equipped with winches and takes a great deal of time, involving the dynamic straightening of the wire as it slowly sinks to the seafloor. Examples of long wire electric field measurements are given in Cox et al. (1971), Filloux (1973), and Webb et al. (1985).

The short span instruments have an electrode spacing of a few meters, utilizing salt bridges (hollow tubes attached to the electrode at one end and the sea on the other) to connect the Ag-AgCl electrodes, which are placed together on the instrument package, to the water. A mechanical device, called a water chopper in Filloux (1974), is used to physically reverse the seawater connection to the electrodes between measurements. This procedure works in a manner similar to electronic chopping amplifiers by moving the operating frequency to a quieter part of the noise spectrum. Chopping also eliminates baseline drift so that the dc electric field is physically interpretable. A major advantage of the short arm instrument is the ease of deployment; it need merely be hoisted over the side of a ship and released. The major disadvantage is the difficulty of fabricating a water chopper that maintains very high resistance isolation of the electrodes, yet operates reliably under the high ambient pressures at the seafloor. Figure 3 shows a short span instrument being deployed from an oceanographic research vessel. This type of instrument is capable of measuring both horizontal electric field components 32 times per hour for 300 days with a least-count value of 0.02 μV/m. Water chopper instruments have recently been developed to measure the vertical electric field for oceanographic studies. The use of a chopper is essential if short span electric field measurements are to be interpretable at periods of an hour or more, as electrode drift can easily dwarf the natural field variations without one.

All of the oceanic MT work performed to date has been done with the purpose of probing the deep lithospheric and asthenospheric structure to depths of hundreds of kilometers (e.g., Filloux, 1981, 1982; Law and Greenhouse, 1981). The data are interpretable in terms of a 1-D conductivity structure in the deep ocean away from continents, and the results indicate low conductivity in the upper 50–100 km followed by an abrupt rise to 0.05–0.2 S/m below this. The resolution of the data is generally quite low (e.g., Oldenburg, 1983), reflecting the strongly band-limited nature of the seafloor EM spectrum. In particular, the data contain little or no information on the conductivity of the oceanic lithosphere above depths of ≈30 km. A possible correlation of the depth to good conductor with lithospheric age has been noted (Filloux, 1980b; Oldenburg et al., 1984), and has been interpreted in terms of partial melting in the presence of water-rich fluids (Tarits, 1986). The ability of MT to resolve lateral changes of structure is better than its sensitivity to vertical variations in conductivity, and array experiments are beginning to exploit this property. The first such effort is the EMSLAB experiment covering the Juan de Fuca plate, and is summarized by EMSLAB Group (1988). The substantial improvement in resolving power from combining both land and seafloor MT data is evidenced by modeling the EMSLAB data, where the top of the subducted Juan de Fuca plate is clearly imaged (Wannamaker et al., 1989). It is likely

that seafloor MT or geomagnetic depth sounding will be especially useful around mid-ocean ridges, where lateral conductivity variations associated with the thermal evolution of the lithosphere are substantial.

In spite of the limitations of the MT method in the oceans, it is presently the only way of obtaining conductivity information from deeper than 30 km or so. The low electrode noise and drift, the homogeneity of the electric fields, and the applicability of the 1-D approximation all help to temper the problem of reduced signal levels. It is unlikely that MT sounding will ever be useful for marine geophysical exploration purposes, except possibly for delineating regional (as opposed to small-scale) geological structure on the continental shelves. However, it must be appreciated that the pioneering electrical work in the ocean was done to obtain information about both the solid earth and about water currents, and that the technology so developed has since been adapted to other more exploration-related purposes.

DIRECT CURRENT RESISTIVITY

The direct current (dc) resistivity method is one of the simplest EM methods available to the explorationist. A direct current is passed into the earth through a pair of source electrodes and the resulting potential difference is measured between another pair of elec-

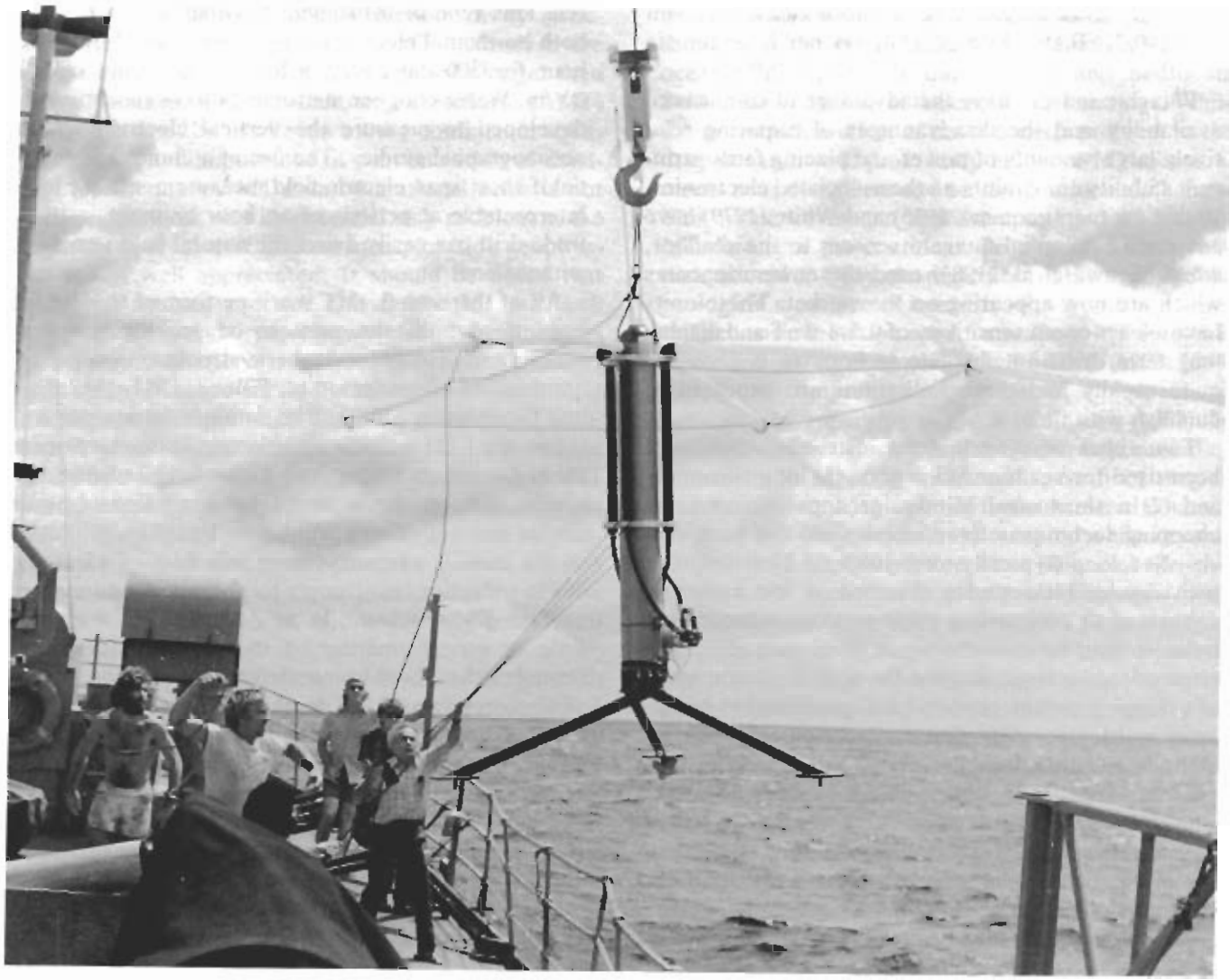

Fig. 3. A short span electric field instrument being deployed from the *R/V Alexander Agassiz* in 1976. The aluminum pressure case houses the recording electronics, while the four horizontal arms are salt bridges that connect Ag-AgCl electrodes, located on the water chopper near the base of the pressure case, to the ocean. The tripod anchor is released under timer control, and the remainder of the instrument returns to the surface under slight positive buoyancy.

trodes. Under the static approximation, electric current has no sources or sinks, and the governing equation is that of conservation of electric current. This is easily solved for simple electrode geometries and electrical structures, and more complicated ones may be treated using numerical approaches.

At a first impression, it appears absurd to attempt the use of dc methods in a highly conducting medium like the ocean because the proportion of the signal which is due to the seabed is given to a first approximation by the ratio σ_1/σ_0, where σ_1 and σ_0 are the conductivities of rock and seawater. This ratio is 0.1 or less in unconsolidated sediments and is further reduced in hard rock. The attenuation becomes even greater if the electrode array is not located on the seafloor (Lagabrielle, 1983). To detect a 10 percent change in the seafloor conductivity requires seafloor-based measurements with a precision of 0.3 percent or better. The requirement for high precision is counteracted in part by the advantages of working in the ocean with potential and transmitter electrodes (low noise and high source current). In spite of these advantages, particular care must be taken in assessing the effects of topography due to the small size of the dc resistivity anomaly in the ocean.

The dc method was developed in France by the Schlumberger brothers between 1912 and 1926, and their brilliance is attested to by the fact that they conducted the first resistivity surveys over water only a few years later (Schlumberger et al., 1934). The object of this work was the determination of seabed structure for a harbor engineering project, and would be accomplished more accurately and inexpensively by acoustic means today. More recent oceanic dc resistivity work has focussed on delineation of sulfide mineral bodies, measurements of extent of submarine permafrost in the arctic, and examination of the porosity structure of the oceanic crust. Neither sulfide bodies nor small porosity changes possess a significant seismic signature, but both have a pronounced effect on electrical conductivity.

Early attempts to use dc techniques to detect the offshore extension of sulfide deposits on the Cornish coast are reviewed in Francis (1985a). More recently, Francis (1977) developed a Wenner array about one-half kilometer in length which was towed on the sea surface for shallow water resistivity sounding in the same area. A source current of 2000 A was provided by the generators of a Royal Navy minesweeper and over 2000 km of survey lines were covered. Bottom profiling by acoustic means allowed correction for the influence of seafloor bathymetry. Several sizable resistivity anomalies were detected which could only be accounted for by sulfide mineralization, but confirmation of the finds by dredging or drilling is lacking.

Francis (1985b) also described a modified Wenner array that can be deployed from a research submersible. A 50 m long cable is towed behind a research submersible and contains both source and receiver electrodes. The unit is weighted to hang vertically below the submarine, and is stretched along the seafloor during the measurement process. The apparatus was designed for the assessment of the massive, polymetallic sulfide ore bodies that have been discovered on mid-ocean ridges. A trial experiment was conducted on the East Pacific Rise in early 1984, and substantial conductivity anomalies were observed around known hydrothermal fields, with local rock conductivity values as large as that of seawater. This should be contrasted with the much lower conductivity (<0.1 S/m) of seawater saturated basalt.

Another related application of a dc method for mineral exploration is proposed in Wynn (1988), who designed a system for the study of induced polarization in titanium-bearing sands. The apparatus consists of a towed 4 Hz dipole source with Ag-AgCl receiver electrodes 30 m in length for use in shallow (≈20 m) water. Preliminary results were inconclusive, primarily due to the lack of a suitable deposit in the test area.

Because of the large electrical conductivity contrast between resistive permafrost and unfrozen sediment, galvanic electrical methods are suitable for the determination of the depth to and thickness of permafrost below the seafloor. Corwin (1983) described the results of a series of trial experiments conducted in an area of known structure off Prudhoe Bay, Alaska, using a 100 m long Schlumberger array towed on the surface behind a small boat. Under good conditions, the method was capable of detecting the depth to permafrost with an accuracy comparable to that of seismic refraction. Resistivity techniques can detect thin permafrost layers quite precisely in shallow water, and can be operated in a rapid, towed, survey mode.

Owing to the relative homogeneity of the upper oceanic crust, large-scale borehole resistivity techniques offer useful measurements of bulk rock conductivity. This technique differs from conventional well-logging because large-scale averages of the conductivity for hundreds of meters around the borehole are obtained, rather than the more typical small-scale values measured by logging tools. The method has been applied in Deep Sea Drilling Project (DSDP) holes which penetrate the basaltic oceanic crust. Neglecting mineralized and hydrothermal zones, the conductivity of surface rocks depends primarily on the degree of water saturation, and hence porosity, and all of the experiments performed to date have been aimed at determining this important parameter.

The experimental set-up for the large-scale resistivity experiment is relatively simple. One current elec-

trode is placed near the surface ship (or maybe the surface ship's hull), while the second is placed near the bottom of the borehole at a depth of 500–1000 m below the seafloor. The potential electrodes are spaced 10–150 m apart, a much larger separation than is used in conventional logging tools, in order to measure conductivity averages over large volumes of rock. This practice practically eliminates the effect of the zone of anomalous resistivity and porosity around the borehole that is produced by the drilling process, and also reduces the influence of small-scale and laterally inhomogeneous structures in the oceanic crust.

Francis (1982) developed the theory and original apparatus for the large-scale downhole resistivity experiment, which was tested in DSDP Hole 459B in the Mariana Basin. While the first trial was only partially successful, it did demonstrate the feasibility of the concept. Two additional experiments have been conducted in DSDP Hole 504B near the Costa Rica Rift south of Panama. Von Herzen et al. (1983) measured the large-scale resistivity to a depth of 836 m below the seafloor during DSDP Leg 70, and several years later, after the hole was extended to nearly 1.5 km depth, the experiment was repeated (Becker et al., 1982; Becker, 1985). Figure 4 shows some results from the latter attempt. The resistivities obtained from the large-scale apparatus agree in form with the results obtained from commercial tools, but are generally lower and smoother because of the averaging properties of the technique and the elimination of drilling disturbance effects on the outcome. The experiment clearly demonstrates an ability to detect the boundary between the uppermost pillow lavas and the deeper sheeted dikes at 850–1050 m below the seafloor. The former have a bulk conductivity as high as 0.1 S/m, while the deeper layer is much more resistive, averaging about 0.005 S/m in conductivity. The resistivity indicates a substantial reduction in porosity from surface values of 7–10 percent to less than 3 percent at depth, and has implications for the depth of hydrothermal circulation

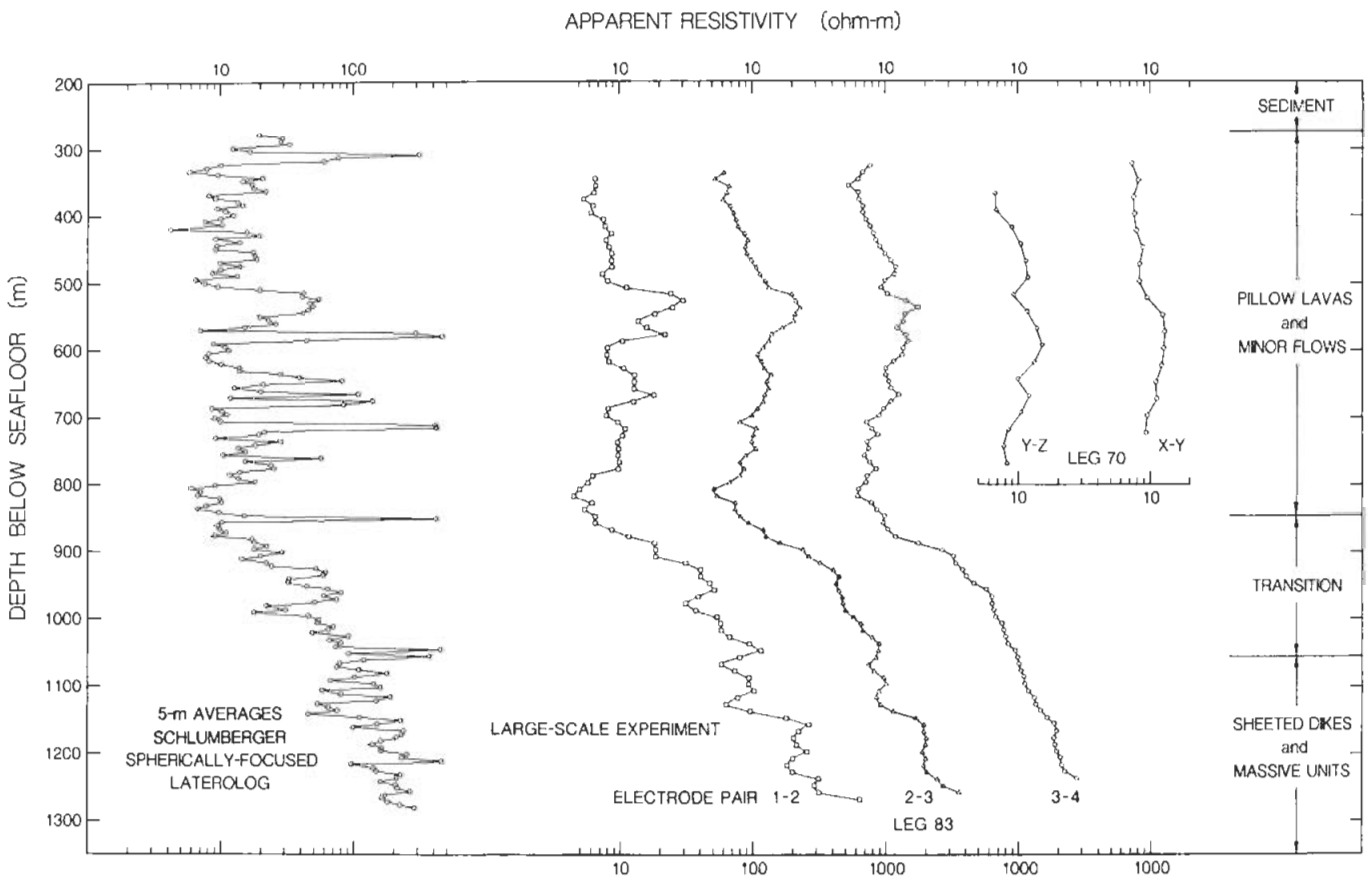

Fig. 4. Large scale resistivity experiment results taken on DSDP Leg 83 and compared to an earlier experiment on Leg 70 and standard logging results. Shown from left to right are 5 m averages of Schlumberger Laterolog resistivities, three independent large scale measurements from Leg 83, and two experiments from Leg 70. All of the traces are plotted on equivalent semi-logarithmic scales and are offset by one decade. The apparent resistivities are about 10 Ω·m in the uppermost pillow lavas and increase to about 1000 Ω·m at the base of the hole (taken from Becker, 1985).

in the oceanic crust. More recently, Becker (1988) described a large scale resistivity experiment from Ocean Drilling Project (ODP) Leg 109 in which a 500 m deep hole in the Atlantic was reoccupied. The results give a different resistivity structure than for Hole 504B, but the inferred porosity structures are similar; this result is attributed to the markedly disparate temperature profiles between the two holes.

MAGNETOMETRIC RESISTIVITY

The principles of the magnetometric resistivity (MMR) method are described by Edwards and Nabighian (this volume). The method is based on the measurement of the low-level static magnetic fields of a grounded electric source. Edwards et al. (1981, 1984) introduced a modification of the method, a natural extension of cross-hole MMR known as MOSES, an acronym which stands for Magnetometric Off-Shore Electrical Sounding. The transmitter is a vertical long-wire bipole extending from the sea surface to the seafloor. A commutated current is fed to two large electrodes: one near the sea surface, the other on the bottom. The return current is through seawater and the subjacent crust. The receiver consists of two orthogonal horizontal magnetic field detectors located on the seafloor. The measured data are two components of the magnetic field as a function of frequency and transmitter-receiver separation.

Accurate estimates of seafloor conductivity are possible using this configuration because the horizontal magnetic field is proportional to the current which enters the crustal material. For dc resistivity sounding, only the value of the TM mode reflection coefficient (equation A-16 in the appendix) at the seafloor, which has a magnitude very close to unity for most crustal conductivities, is obtained. By contrast, the MOSES method measures the transmission coefficient $1 + R_L^{\mathrm{TM}}$ which, in the static limit, is proportional to the crustal conductivity. The principle is illustrated in Figure 5. Ampere's circuital law is applied to a horizontal path on the seafloor, centered at the base of the current bipole. The total current flow, for a uniform sea layer above a uniform layered earth, has axial symmetry about a vertical line defined by the bipole. The azimuthal magnetic field is constant in magnitude around the Ampere circuit and is due only to the current which crosses its plane (i.e., the current which enters the seafloor). This current may be shown to be proportional to the ratio of the sediment conductivity to that of seawater. Consequently, the associated magnetic field is a direct measure of the basement conductivity.

The azimuthal magnetic field B_ϕ in the quasistatic limit is given by

$$B_\phi = \frac{\mu_0 I}{2\pi} \int_0^\infty dk\, J_1(k\rho)\, \frac{k^2}{\beta^2}\, \frac{1 + R_L^{\mathrm{TM}}}{2} \times \left[\frac{1 - 2e^{-\beta H} + e^{-2\beta H}}{1 + R_L^{\mathrm{TM}}\, e^{-2\beta H}} \right] \tag{6}$$

where β is given by equation (A-17) in the appendix, I is the source current, ρ is the source-receiver range, and H is the water depth. The seafloor can be modeled as a half-space of conductivity σ_1 and approximate solutions can be obtained for the case σ_1 small compared with the seawater conductivity σ_0 can be derived. A simple useful formula can be obtained provided two additional approximations are made. First, the range ρ must be large compared to the depth of the ocean H. Second, the integrated conductivity of the sea layer $\sigma_0 H$ must be large compared with the parameter product $\sigma_1 \rho$, so that the bipole current is channeled out to relatively large distances by the sea layer. At the static limit, a simple expression for the azimuthal magnetic field results

$$\beta_\phi = \frac{\mu_0 I \sigma_1 H}{4\pi\sigma_0 \rho^2} (1 - i\omega\mu_0\sigma_1\rho^2/2). \tag{7}$$

Computations and graphs presented in the theoretical papers already referenced indicate that the field strength is small. However, the field need only be measured to an accuracy of 10 percent to obtain the seafloor conductivity to the same degree of approxi-

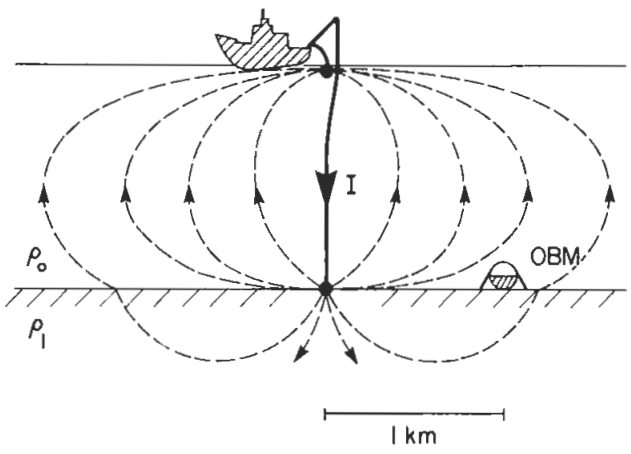

MOSES

Fig. 5. Schematic illustrating the principle of the MOSES method. The current flow is axisymmetric about the bipole source. The relatively small amount of current entering the resistive crust is proportional to the ratio of the crustal to seawater conductivities. By Ampere's circuital theorem, only this current contributes to the azimuthal magnetic field measured at a point on the seafloor.

mation. Estimates of seafloor conductivity are obtained at all transmitter-receiver separations, with the larger spacings yielding averages encompassing greater depths.

In the static limit, apparent resistivity curves similar to standard Schlumberger sounding curves without the sea layer may be constructed to aid in layered earth interpretations. Traditionally, an apparent resistivity formula is a function of the actual field measurements multiplied by a numerical factor derived for the special case where the ground volume studied is homogeneous and isotropic. In the MOSES case, no simple formula that is valid over a wide range of model parameters exists. Expression (7) for the field B_ϕ, with frequency ω set equal to zero, may be inverted to yield a formula used to transform field data into a domain where they may be compared with model curves for the whole range of parameters encountered. The apparent resistivity formula is

$$\rho_a = \frac{\mu_0 I H}{4\pi\sigma_0 \rho^2 B_\phi} . \tag{8}$$

The expression reduces exactly to the resistivity of a half-space beneath the sea only when the conditions for the validity of expression (7) hold. A suite of apparent resistivity curves for a layer over a half-space is shown in Figure 6.

Experimental MOSES systems have been developed for deep crustal sounding (Edwards et al., 1985; Nobes et al., 1986), for mapping sulfide deposits in the vicinity of mid-ocean ridges (Wolfgram et al., 1986), and for determining the physical properties of permafrost beneath the Beaufort Sea (Edwards et al., 1988). The apparatus for a MOSES experiment depends on the application, but in general divides into two broad categories: (1) that required to perform the actual sounding, and (2) that required to determine position at sea.

Of particular interest are the designs of the seafloor magnetic receivers which are described briefly. For deep crustal sounding experiments, the seafloor receiver is the remote microprocessor controlled device shown in Figures 7 and 8. The receiver is dropped in free fall from a surface vessel. On deployment, the shape of the anchor ensures a landing within one or two degrees of the vertical in well-sedimented regions. At some preprogrammed later time, it releases its anchor and returns to the sea surface. The sensors consist of two orthogonal, horizontal component fluxgate magnetometers based on the Scintrex MFM3 design. The inherent noise level of each sensor is $4\text{pT}/\sqrt{\text{Hz}}$ at 1 Hz. However, when operated close to the other electronic equipment forming the receiver, the noise level increases almost tenfold. Magnetic fields detected by the magnetometers are filtered, digitized, stacked, and recorded in solid state memory under the control of a microprocessor. The bucking of the fluxgate instruments and the timing of all experimental operations are also under software control.

The first successful sea test of a MOSES system is described in Edwards et al. (1985). The test area, Bute Inlet, is located approximately 200 km NW of Vancouver, British Columbia, Canada. The inlet is more than 50 km long and averages 3 km in width. It is a vee-shaped valley containing seawater about 650 m deep overlying sediment estimated to be 600 m thick by extrapolating the shape of the adjacent topography downward beneath the sea.

The field data in Figure 9 were used to compile the apparent resistivities and associated errors shown in Figure 10 taken along an axial profile down the inlet. The range of separation of the transmitter and receiver is 150–2000 m. The averaging time at each station was 1 h. The operating frequency was 0.125 Hz, which is just low enough to allow the effects of induction to be

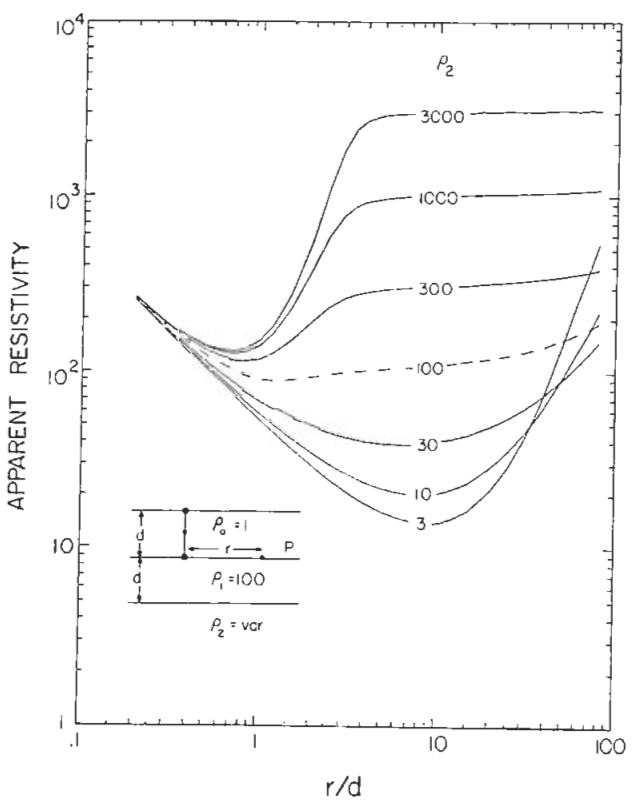

Fig. 6. MOSES apparent resistivity curves for the model of a layer over a half-space beneath the sea as a function of the source-receiver offset normalized by the water depth. The layer is assumed to have a thickness comparable to the depth of the ocean and a resistivity contrast of 100 with the ocean. The resistivity contrast with the lower half-space is variable as marked.

neglected. Errors in apparent resistivity at short spacings are principally due to uncertainty in position, whereas those at large separation are due to errors in magnetic component estimation.

The local geology beneath the sea can be modeled by one layer over a half-space. The layer represents the conductive sediment and the half-space the relatively resistive basement rock. The best fitting model is inset into Figure 10; the corresponding type curve is shown as a very heavy line. An independent estimate of the coarse error bound (Jupp and Vozoff, 1975) in both the layer conductivity and thickness is calculated as 9.2 percent. The error in the half-space resistivity is illustrated by plotting the family of type curves shown in Figure 10. By inspection, the ratio of resistivities ρ_h/ρ_c between the lower half-space and the layer must be at least 10 and could be larger. The estimates of the sediment thickness and resistivity determined by the technique are reasonable. The sediment resistivity of 1.9 $\Omega \cdot$m corresponds to a porosity of about 42 percent, which is in the range of that measured on core samples. The thickness of the sediments, estimated at 560

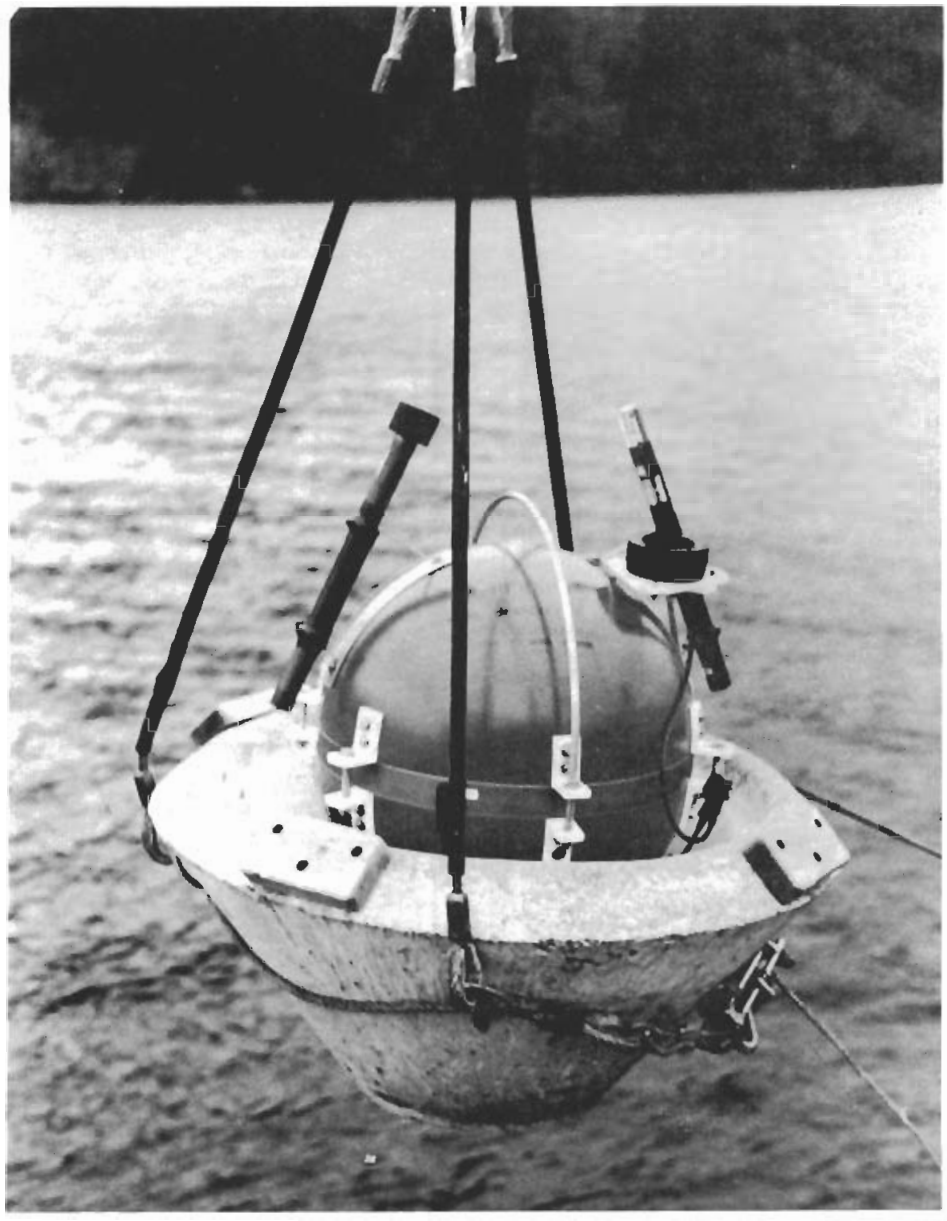

Fig. 7. The MOSES deep water receiver mounted in its concrete anchor. The instrument is housed in a spherical aluminum pressure case that floats to the surface when the concrete base is released. A 27 MHz radio beacon and a flasher unit are attached to the left and right sides of the pressure case, respectively, as an aid in instrument recovery. The small black circular ring in front of the strobe is an acoustic transponder.

m, is less than the upper estimate of 600 m obtained by extrapolating the shape of the adjacent topography downward beneath the sea. The value is also in good agreement with that obtained by reflection seismology. The interpreted range of basement resistivity does include that of typical crystalline rock.

The MOSES method has also been used in deep water. Nobes et al. (1986) determined the resistivity and porosity of the sediment and fractured basalt layers in the Middle Valley of the northern Juan de Fuca Ridge system. The valley is generally flat and featureless. Two sites within the valley were studied; the first site is in the central region, which is filled with a thick sequence of clay turbidites, while the second site is in the southern region, where the sediments are much thinner. A geologically reasonable model for both sites is a relatively conductive layer representing the sediment overlying a relatively resistive half-space approximating the fractured basalt. When this model is fit by least squares to site 1 data, the sediment thickness and resistivity are obtained as $0.82 \pm 0.06\ \Omega\cdot m$ and 1800 ± 300 m, respectively. The sediment porosity which corresponds to the quoted resistivity is of the order of 30 percent. The resistivity of the fractured basalt is indeterminate. When the same model is adjusted to fit site 2 data, the thickness of the sediment is obtained as 200 ± 50 m on average provided the resistivity of the layer is specified as that determined at site 1. The resistivity of the basalt is 30 percent higher at a value of $8.5 \pm 3.4\ \Omega\cdot m$, corresponding to a porosity of about 8 percent. The fractured zone is at least 1000 m thick.

The field technique used in the Arctic experiments was very different from that previously described, and

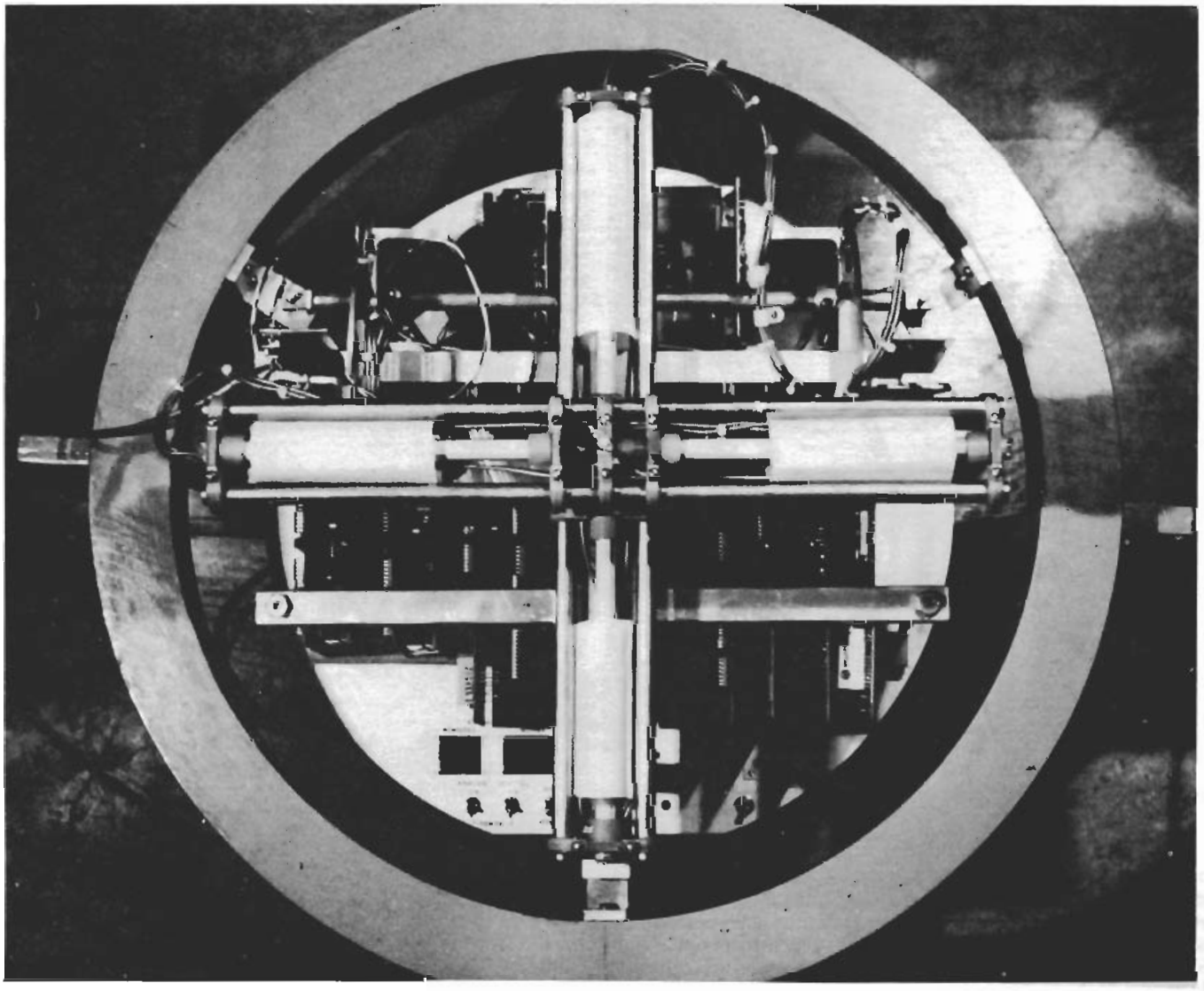

Fig. 8. The interior of the MOSES deep water receiver showing the two orthogonal fluxgate magnetometers and the microcomputer boards.

the design of the sensor reflects this. The instrumentation had to be lowered and subsequently recovered through a 10 inch hole in the sea ice which covers the surface until the late spring of every year. The ice sometimes forms a very stable floating platform for geophysical experiments. The sensor, shown in Figure 11, is folded up and lowered vertically into the hole. It is rigged to unfold on passing through the hole to form the horizontal square framed arrangement shown in the figure. The unit is then gently lowered to the seafloor. The field sensors are coils wound on a soft iron laminated core and are contained in stainless steel jackets. The coil and its current amplifier have a flat frequency response from 0.5 to 200 Hz.

The Arctic experiment (Edwards et al., 1988) represents the first application of MOSES to a problem of importance to the petroleum industry. The target is the permafrost layer under the Beaufort Sea, a seismically rigid layer from 100–600 m thick underlying shallow water typically 10–100 m deep. Detailed knowledge of the location and physical properties of the permafrost layer is essential for accurate interpretation of seismic reflection data. The permafrost can contain pockets of gas hydrate. The gas hydrate is both a possible resource and a hazard to drilling operations. A local map of the permafrost zone is essential geotechnical information required prior to the construction of an offshore structure or pipeline.

The test sounding was conducted northwest of Tuktoyaktuk at the location marked with a cross on Figure 12. The depth of water beneath the ice at the site was only 16 m, a little too shallow to demonstrate the full potential of the technique. The data are displayed in the form of magnetic field amplitude and phase shift curves in Figure 13. The interpretation was accomplished using an algorithm developed in Constable et al. (1987). The method seeks to minimize the roughness of the conductivity-depth profile, defined as the integrated square of either the first or second derivative of the profile. The two curves that result are shown in Figure 14. The resistivity clearly increases rapidly with depth. The profiles are consistent with a two-layer model of the seafloor composed of soft recent marine sediments with a porosity in excess of

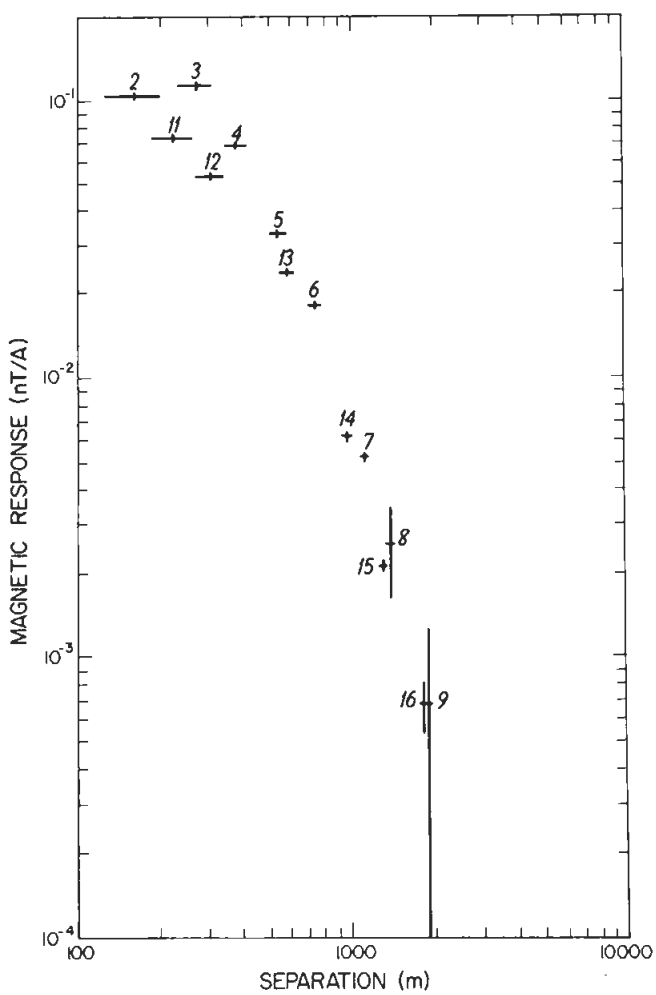

Fig. 9. The azimuthal magnetic field amplitude at a frequency of 0.125 Hz as a function of transmitter-receiver separation for the Bute Inlet MMR experiment described by Edwards et al. (1985). The magnetic field is normalized by the transmitter current and plotted as a function of transmitter-receiver separation. The numbers correspond to the sites where measurements were made; see Edwards et al. (1985) for details.

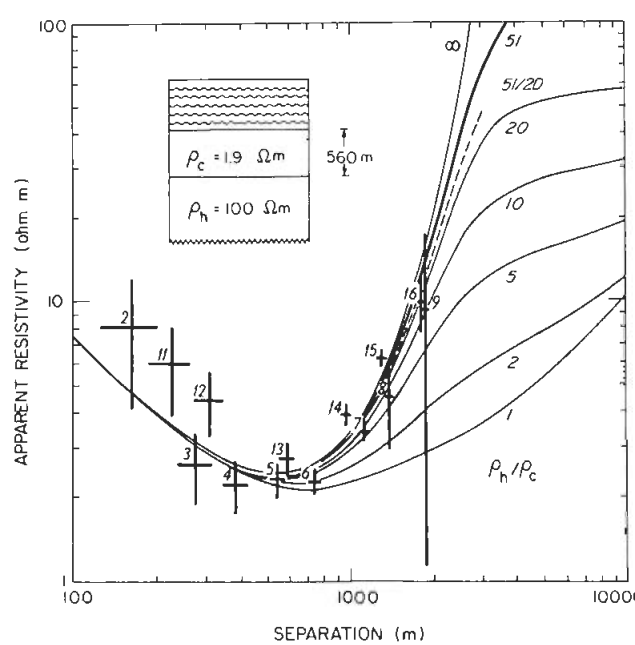

Fig. 10. The apparent resistivity as a function of transmitter-receiver separation for the Bute Inlet MMR data of Figure 9. The curves are for the model of a layer over a more resistive halfspace beneath the sea shown in the inset. The numbers correspond to the measurement sites of Figure 9.

35 percent overlying deltaic sands of lower porosity which are probably partially frozen.

SELF POTENTIAL

The measurement of electric self potential (sometimes called spontaneous polarization or SP) is an established method of geophysical prospecting on land and is used primarily in the search for sulfide mineral deposits. The origin of SP fields is not certain. The most acceptable mechanism is that of Sato and Mooney (1960) who suggest that SP fields result from electric currents that are produced when a conducting body connects regions of different electrochemical potential. Seawater has a reduction-oxidation (redox) potential (Eh) of +200 to +400 mV, while marine sediments have Eh values of −100 to −200 mV a small distance below the water-sediment interface, and the seafloor serves as a strong redox boundary. A conducting object, such as a mineral deposit, that pierces the contact will produce an electric current; the return current occurs in a diffuse zone surrounding the body, causing an SP anomaly.

Corwin (1975) has examined the principles of SP prospecting in the ocean, and notes the advantages already discussed of using electrical methods in the ocean. It is convenient to tow a pair of electrodes through the ocean, making rapid SP surveys of large areas quite feasible. SP apparatus is very simple, consisting of a pair of nonpolarizing potential electrodes and a recording voltmeter. However, as for the dc method, the SP effect is reduced by a factor of σ_1/σ_0, where σ_1 and σ_0 are the conductivities of sediment and seawater, but this attenuation is not large where the near-bottom marine sediments are water saturated and have an electrical conductivity approaching that of seawater.

Corwin (1975) reports that wave- and tow-induced potentials are the most significant types of contamination in oceanic SP. Surface wind waves and swell produce EM noise both by direct induction and by producing periodic motion (strumming) of cables that are moved through the earth's magnetic field. Both of these are high frequency, narrow-band processes, and can be reduced substantially by filtering. Tow noise is

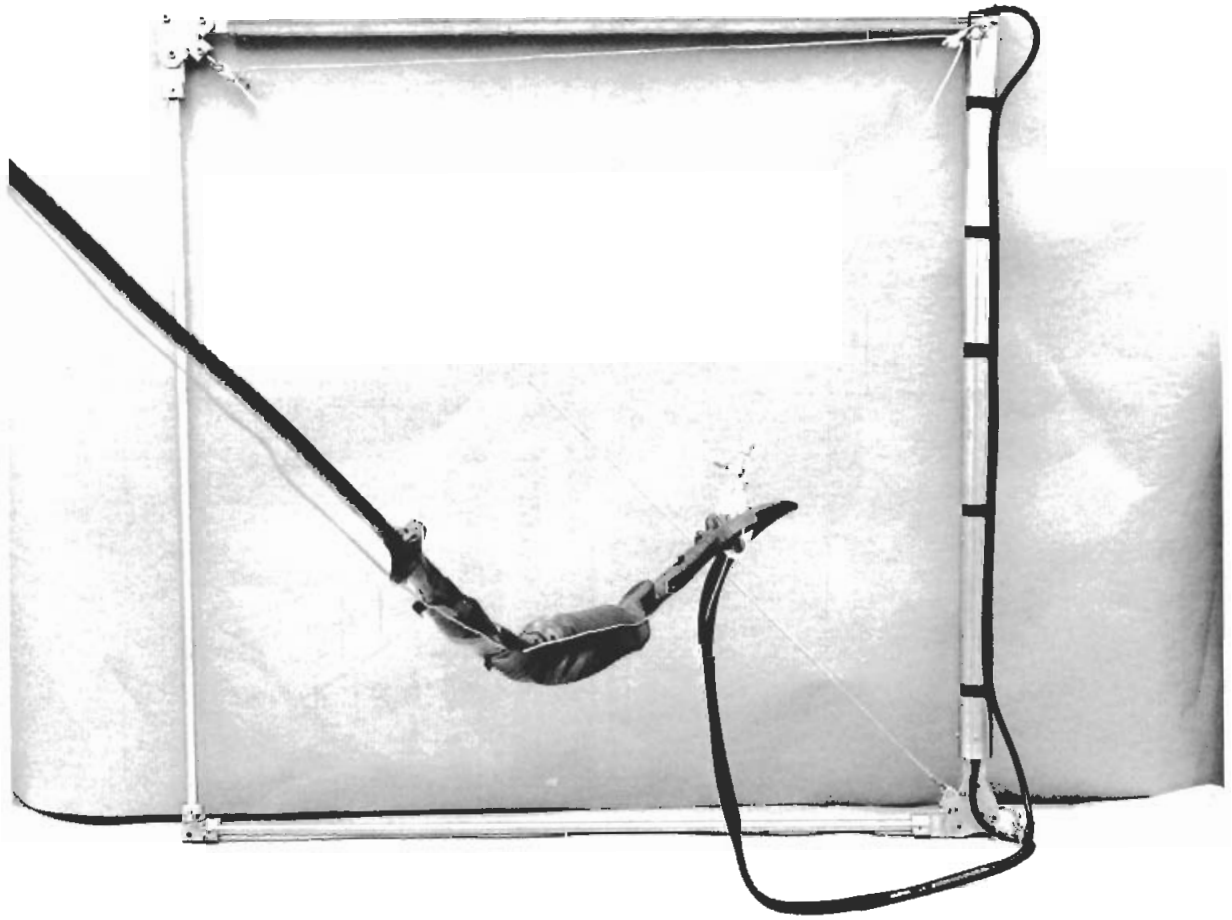

Fig. 11. The ICE-MOSES folding sensor.

caused by changes in the nearly dc potential produced by moving a conducting cable through the geomagnetic field when the heading is altered. This noise is large only during turns, and can be corrected by careful navigation. Turbulence is another likely source of background noise. However, noise levels below the millivolt level have been obtained, so that SP anomalies of only a few millivolts can be differentiated from spurious effects.

Corwin et al. (1970) and Corwin (1975) describe an apparatus designed to be towed at the sea surface for shallow water SP surveys. The first apparatus uses salt bridges to connect shipboard Ag-AgCl electrodes to the ocean and measures the vertical potential difference. The second design uses Ag-AgCl electrodes at the ends of conducting cables and separated horizontally by 10–100 m. Both units record the SP potential on shipboard, and are towed at speeds of 5–10 knots. Brewitt-Taylor (1975) has developed an SP apparatus that is towed a short distance above the seafloor for use in the deep ocean. A pair of Ag-AgCl electrodes were placed on a weighted streamer 50 m apart and connected to a near-bottom recording package. More recently, Schultz (pers. comm., 1988) has described three-dimensional (3-D) model studies of sulfide ore bodies on the mid-ocean ridge, and suggested that simultaneous measurement of the horizontal and vertical gradient fields offers real advantages.

The number of oceanic SP surveys performed to date is quite limited. Corwin (1975) describes the results of shallow water (<20 m) surveying in Penobscot Bay, Maine, in which the offshore extension of known land sulfide mineral deposits were successfully detected, with SP anomalies as large as 300 mV. Brewitt-Taylor's (1975) deep ocean trials were inconclusive. With the interest that seafloor sulfide mineralization is arousing, it is probable that SP will be applied more frequently in coming years.

CONTROLLED SOURCE EM METHODS

Controlled source EM methods utilize time-varying electric and magnetic dipole sources of known geometry to induce electric currents inside the conducting earth. The electric or magnetic signature of the currents can be detected and can yield a measure of the electrical conductivity of the underlying rock. The four fundamental source/receiver types for controlled source work are the vertical and horizontal electric dipoles (VED and HED) and the vertical and horizontal magnetic dipoles (VMD and HMD), and there are many practical combinations of them.

The earliest development work on seafloor con-

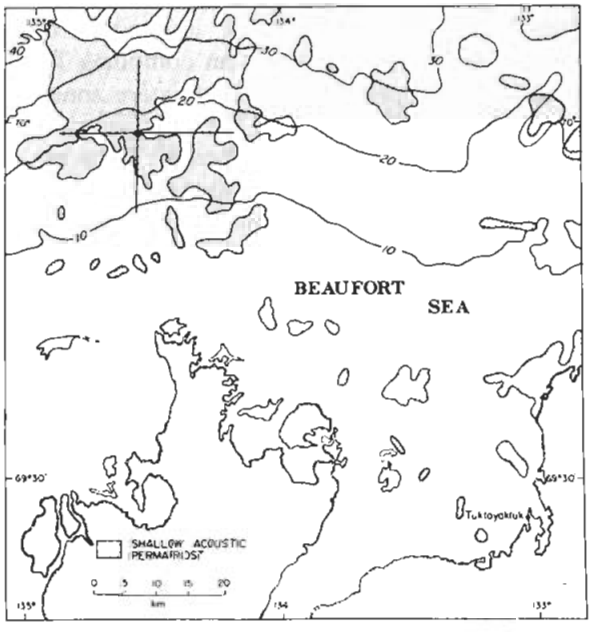

Fig. 12. The location of the Beaufort sea sounding (marked by the cross at upper left) superimposed on a regional map. The shaded areas indicate where permafrost has been mapped acoustically. The water depth contours in feet are also shown.

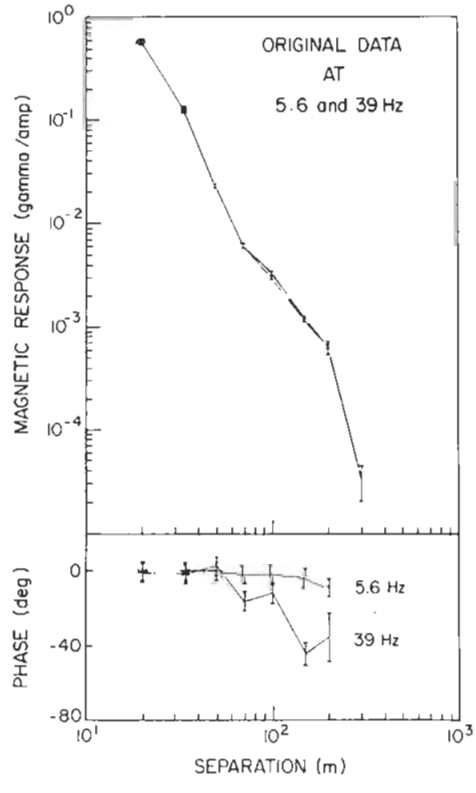

Fig. 13. The magnetic field amplitude and phase at two frequencies as a function of transmitter-receiver separation for the Beaufort sea experiment. The magnetic field has been normalized by the source current.

trolled source systems appears to be due to Drysdale (1924), who describes an extensive program to measure the magnetic field and electric current around a submarine cable for use in a ship guidance system of World War I vintage, and shows that many of the difficulties of working in the ocean have not changed over time. In an accompanying paper, Butterworth (1924) computed the fields about the cable and over an insulating seafloor for comparison to the measurements. More recently, Bannister (1968a, 1968b) calculated the seafloor fields produced by an extended HED placed on the sea surface and a seafloor HMD, both with the purpose of determining the seabed conductivity. Coggon and Morrison (1970) modeled a seafloor VMD source with both electric and magnetic receivers, emphasizing exploration of the uppermost few hundred meters of the seabed. Kaufman and Keller (1983) computed seafloor sounding curves for VMD and HED sources with a vertical magnetic field receiver.

Oceanic controlled source problems differ from their terrestrial counterparts in important ways: both source and receiver are always immersed in a conductive medium, and the electrical structure both below and above the medium influences the induction problem. Furthermore, some system geometries require the explicit inclusion of the ocean-atmosphere boundary in the theory. The importance of interactions with the sea surface when using seafloor-based controlled source systems in electrically shallow water is discussed in Coggon and Morrison (1970) and Chave and Cox (1982), and will be especially important on the continental shelves. The finite depth of the ocean may be neglected at frequencies where the water is many skin depths deep if the source-receiver separation is small enough.

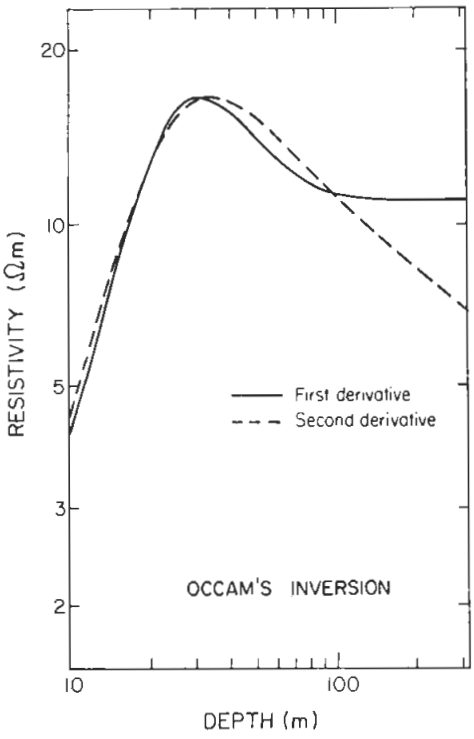

Fig. 14. The inversion of the Beaufort sea data to continuous resistivity/depth models of minimum slope and minimum second derivative (curvature), respectively.

TM and PM modes can be associated with the four basic types of sources: (1) the vertical electric dipole (VED) generates only TM modes, (2) the vertical magnetic dipole (VMD) induces only PM modes, and (3) the horizontal electric dipole (HED) and (4) horizontal magnetic dipole (HMD) are more general, and can produce both modes. An EM exploration system is made up of some source-receiver combination. It is of no use to generate a desirable mode with the source if the receiver is incapable of detecting it. For this reason, symmetric systems in which the source and receiver are of the same type are commonly used. In our notation, when HED, VMD, and HMD refer to systems, they are the collinear horizontal electric dipole-dipole, coplanar vertical magnetic dipole-dipole, and coaxial horizontal magnetic dipole-dipole combinations.

The theory associated with controlled source methods for terrestrial exploration is well-understood (e.g., Spies and Frischknecht, this volume) and the theoretical properties of some common systems on land can be grouped as follows. The VMD and HMD types detect only horizontal current flow (PM modes) in a 1-D earth, hence are relatively insensitive to thin resistive zones. The HED system combines TM and PM modes and is preferred when resistive zones have to be mapped. The grouping of these three systems on the seafloor is fundamentally different. They are now buried inside a conductive medium rather than lying on a conductive half-space, and preconceptions based on their terrestrial use can be quite misleading. The VMD system still is based only on a PM mode, but the HED and HMD systems generate and receive both PM and TM modes. Furthermore, the secondary EM fields due to induction in the crustal material are measured near the interface of a good conductor (seawater), so a system like the VMD, in which a component of a field which vanishes at the surface of a good conductor is measured, is unlikely to display sensitivity to a resistive seafloor. This is not true for the HED and HMD systems, which are both quite capable of accurately measuring the conductivity of the seafloor in the common instance where seawater is more conductive than rock. The less common circumstance of a relatively conductive seafloor is analogous to the terrestrial case, and systems like the VMD type are then sensitive to seafloor conductivity.

The choice of operating an EM system in either the

frequency domain, transmitting a set of discrete frequencies one or a few at a time, or the time domain, transmitting a square or triangular step and measuring the transient response of the seafloor-ocean system, also exists. The physics of the two methods are identical, the response in one domain being the Fourier transform of the response in the other domain. Because of the finite and inexact nature of practical measurements, this transformation cannot usually be made outside the realm of theoretical studies. The choice of one system over another must be made on the basis of practical and logistical considerations.

Frequency Domain EM

Chave and Cox (1982) developed the theory for the frequency domain HED method using the modal formulation given in the appendix, and some details will be summarized to illustrate the behavior of frequency domain controlled source EM (CSEM). Only the electric field will be considered here. Using the Green functions from equations (A-14) and (A-15), taking the limit of an infinitely deep ocean ($H \to \infty$), and utilizing the cylindrical symmetry to convert from a Fourier to a Hankel transform, the radial, azimuthal, and vertical electric fields may be written

$$E_\rho = \frac{p}{4\pi\sigma_0}\cos\phi\int_0^\infty dk\left\{J_0(k\rho)k\beta R_L^{\mathrm{PM}} - \frac{1}{\rho}J_1(k\rho)\times\left[\beta R_L^{\mathrm{TM}} + \frac{\gamma_0^2}{\beta}R_L^{\mathrm{PM}}\right]\right\}e^{-\beta(z+z')} - \frac{p}{4\pi\sigma_0}\cos\phi\int_0^\infty dk\left[J_0(k\rho)k\beta - \frac{1}{\rho}J_1(k\rho)\frac{k^2}{\beta}\right]e^{-\beta|z-z'|} \quad (9)$$

$$E_\phi = \frac{p}{4\pi\sigma_0}\sin\phi\int_0^\infty dk\times\left[J_0(k\rho)\gamma_0^2\frac{k}{\beta}R_L^{\mathrm{TM}} - \frac{1}{\rho}J_1(k\rho)\left[\beta R_L^{\mathrm{TM}} + \frac{\gamma_0^2}{\beta}R_L^{\mathrm{PM}}\right]\right]e^{-\beta(z+z')} + \frac{p}{4\pi\sigma_0}\sin\phi\int_0^\infty dk\times\left[J_0(k\rho)\gamma_0^2\frac{k}{\beta} + \frac{1}{\rho}J_1(k\rho)\frac{k^2}{\beta}\right]e^{-\beta|z-z'|} \quad (10)$$

$$E_z = -\frac{p}{4\pi\sigma}\cos\phi\int_0^\infty dk\,J_1(k\rho)k^2\times[R_L^{\mathrm{TM}}e^{-\beta(z+z')} \mp e^{-\beta|z-z'|}] \quad (11)$$

where p is the source dipole moment in A-m, ϕ is the azimuthal angle measured with respect to the source, ρ is the horizontal range, z and z' are the receiver and source heights, R_L^{TM} and R_L^{PM} are the seafloor modal reflection coefficients given by equation (A-16), β is given by equation (A-17), and γ_0 is the self-induction parameter given by equation (4). The upper sign in equation (11) holds for $z > z'$ and vice versa. The first terms in equations (9)–(11) represent propagation in the underlying rock and along the sea-rock interface, while the second terms, which can be evaluated in closed form (Chave and Cox, 1982, Appendix B), represent propagation in the ocean. The electrical conductivity structure beneath the seafloor enters the problem only through the reflection coefficients R_L^{TM} and R_L^{PM}, and equations (9)–(11) are wavenumber expansions of the fields.

It is helpful to model the seafloor as a half-space of conductivity σ_1 and obtain approximate analytic solutions to equations (9)–(11) for $\sigma_1 \ll \sigma_0$. The reflection coefficients, equation (A-16), are expanded in powers of σ_1/σ_0, and only the lowest order terms are retained. Letting the source and receiver both occupy the interface ($z = z' = 0$) and evaluating the Sommerfeld-type integrals yields the horizontal components

$$E_\rho \approx \frac{p}{2\pi\sigma_0}\cos\phi\left[\frac{(\gamma_0\rho+1)}{\rho^3}e^{-\gamma_0\rho} + \frac{(\gamma_1^2\rho^2+\gamma_1\rho+1)}{\rho^3}e^{-\gamma_1\rho}\right] \quad (12)$$

$$E_\phi \approx \frac{p}{2\pi\sigma_0}\sin\phi\left[\frac{(\gamma_0\rho+1)}{\rho^3}e^{-\gamma_0\rho} + \frac{2(\gamma_1\rho+1)}{\rho^3}e^{-\gamma_1\rho}\right] \quad (13)$$

where γ_1 is equation (4) with σ_1 substituted for σ_0. To get an expression for the vertical electric field, an additional approximation discussed in Cheesman et al. (1987) and valid at ranges comparable to or larger than a skin depth in the lower medium must be invoked, yielding

$$E_z \approx \frac{p}{2\pi\sigma_0}\cos\phi\frac{\sigma_1}{\sigma_0}\frac{\gamma_0(\gamma_1\rho+1)}{\rho^2}e^{-\gamma_1\rho}. \quad (14)$$

Note that equations (12) and (13) are lowest order in σ_1/σ_0, but equation (14) is a first order term, so that any observed vertical electric field indicates a nonzero seafloor conductivity, as is required by conservation

of electric current. The first terms in equations (12) and (13) correspond to a disturbance propagating in the ocean and along the seafloor, and vanish rapidly for $\rho \gg |\gamma_0|^{-1}$. For a frequency of 1 Hz, the seawater skin depth is 270 m, and the oceanic component is negligible beyond about 1 km. By contrast, the second terms correspond to a similar disturbance below and along the seafloor, and attenuate much more slowly with range, dominating the solution when $\rho \gg |\gamma_0|^{-1}$. For ranges $\rho \approx |\gamma_1|^{-1}$, the field decays slowly (as ρ^{-1} to ρ^{-3}), while at larger ranges the exponential term controls the attenuation. This can be contrasted to the terrestrial case, where the disturbance propagating in the low conductivity air is much larger than the geophysically useful one in the underlying rock at all ranges.

Figure 15 shows the radial and vertical electric fields, obtained by integrating equations (9) and (11) numerically, as a function of source-receiver separation at a frequency of 1 Hz and for an ocean half-space of conductivity 3.2 S/m overlying rock half-spaces of conductivity 0.05 and 0.005 S/m. The behavior of the azimuthal electric field is similar to that of the radial part except for the different angular dependence seen in equations (9) and (10). The skin depths corresponding to the conductivities are 270 m in seawater and 2.3 or 7.1 km in rock. At ranges below a skin depth in the lower medium, the source looks like a quasi-static dipole, and the horizontal electric field attenuation is largely controlled by the conductivity of the ocean. At a range of about one skin depth, the effect of the lower half-space becomes noticeable, but the conductivity dependence of the field is weak and the attenuation is not sharp. At larger ranges, the attenuation becomes exponential as in equations (12) and (13), so that the differences between the two models increase as the offset grows. By contrast, the vertical electric field is sensitive to the lower medium conductivity in the quasi-static limit, as seen in equation (13), and a smaller rock conductivity results in weaker fields. At even larger ranges, propagation effects yield more rapid attenuation as the seafloor conductivity increases. The vertical electric field is always substantially smaller than the horizontal components when the ocean conductivity exceeds that of the underlying rock. By the reciprocity theorem, the vertical electric field produced by an HED is equivalent to the azimuthal electric field generated by a VED, so that the HED always yields larger fields for a given range, frequency, and source dipole moment. However, it is clear from Figure 15 that the vertical electric field is sensitive to the conductivity of the half-space at smaller ranges, and that the relative changes in amplitude of the vertical and horizontal electric fields are comparable for a given change in the medium conductivity.

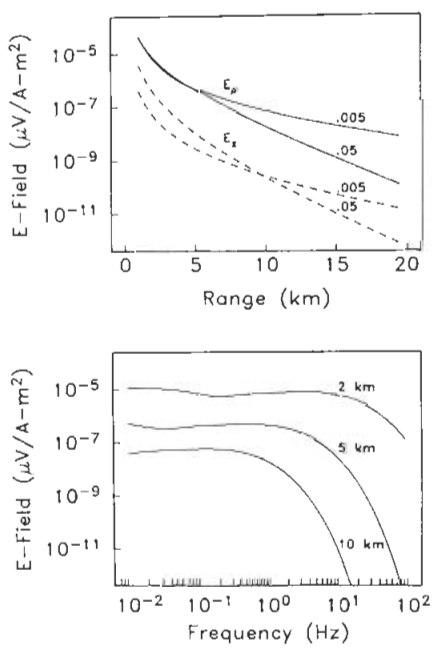

Fig. 15. The upper panel shows the radial and vertical electric fields per unit of source dipole moment as a function of range at a frequency of 1 Hz and for lower half-spaces of conductivity 0.05 and 0.005 S/m. The lower panel shows the radial electric field as a function of frequency at ranges of 2, 5, and 10 km for a lower half-space of conductivity 0.05 S/m. The ocean conductivity is taken as 3.2 S/m, and the radial electric field is measured off of the end of the source.

Figure 15 also shows the radial electric field as a function of frequency for several ranges and a lower half-space of conductivity 0.05 S/m. At frequencies corresponding to skin depths larger than the source-receiver spacing, the behavior is that of a static dipole, with only slight attenuation as the frequency rises. The attenuation and attenuation rate increase at frequencies corresponding to skin depths smaller than the range. The phase of the electric field (not shown) behaves similarly, with attenuation at a radian per skin depth at long ranges and high frequencies and little variation at the other extreme. Similar relationships exist for the magnetic field components; see Chave and Cox (1982) for details.

It is instructive to examine the behavior of the horizontal electric field for geometric (range-dependent) and parametric (frequency-dependent) soundings in the presence of the simplest structural complication, a buried layer. In each case, a specific model consisting of a half-space of conductivity 0.05 S/m containing 1 km thick layers either ten times more or less conductive and centered at depths of 1.5 and 5.5 km is considered; these values are intended only to be illustrative. Figure 16 shows the geometric sounding

curves. The low conductivity zone behaves as a lossy waveguide which traps and guides the signal, resulting in slower attenuation with range when compared to the half-space case. The deep buried layer produces a smaller effect, as expected from the diffusion nature of EM induction, and requires a larger range for the trapping to become apparent. If the buried layer has a higher conductivity than the surrounding material, greater attenuation will ultimately result at long range, but the low conductivity waveguide created between the seafloor and the layer results in an increase in signal strength at intermediate distances. The HED method is preferentially sensitive to relatively low conductivity zones due to the presence of the TM mode. The existence of a minimum usable source-receiver spacing of 1–3 times the burial skin depth, depending on the sense of the conductivity contrast, is also apparent. Longer ranges are required to detect low conductivity material. Figure 17 shows parametric sounding curves for the same model at ranges of 5 and 10 km. The relationships discussed for Figure 16 are observed, with the greatest sensitivity to high conductivity zones occurring at frequencies corresponding to the skin depth that equals the range, while the low conductivity zone is sensed at the largest ranges and highest frequencies.

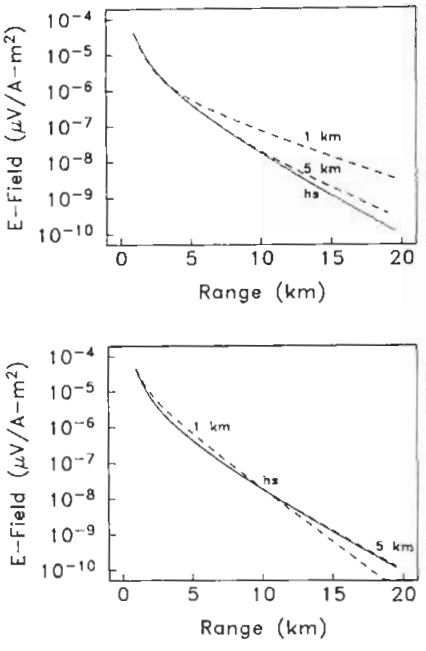

Fig. 16. The radial electric field as a function of range at a frequency of 1 Hz for an ocean half-space of conductivity 3.2 S/m and a lower half-space of conductivity 0.05 S/m containing 1 km thick layers at 1 and 5 km depth. In the upper panel the layers have a low relative conductivity of 0.005 S/m, while in the lower panel the conductivity of the layer is high (0.5 S/m).

Time Domain EM

The increasing interest in time-domain EM (TEM) systems for terrestrial mineral exploration led Edwards and Chave (1986), Cheesman et al. (1987), and Edwards and Cheesman (1987) to investigate the response of a variety of seafloor transient systems. Figure 18 illustrates the TEM response for a coaxial HMD system in the simple case of a uniformly conducting seafloor half-space. The HED response behaves in a qualitatively similar way. For these two systems, and when the seafloor is more resistive than seawater, the position in time of the initial rise of the step-on transient is indicative of the conductivity of rock. A second, later transient is a measure of the conductivity of seawater, and the ultimate measured field is just the steady-state, dc value. The sense of the separation of the parts of the transient is opposite to that in air, where the direct part propagating in the atmosphere arrives almost instantaneously. The quantities plotted in Figure 18 are the dimensionless magnetic fields obtained by normalizing the transient by the late-time dc response, and the dimensionless time, obtained by normalizing the actual time by the EM diffusion time constant in seawater given by

$$\tau_0 = \mu_0 \sigma_0 \rho^2 \qquad (15)$$

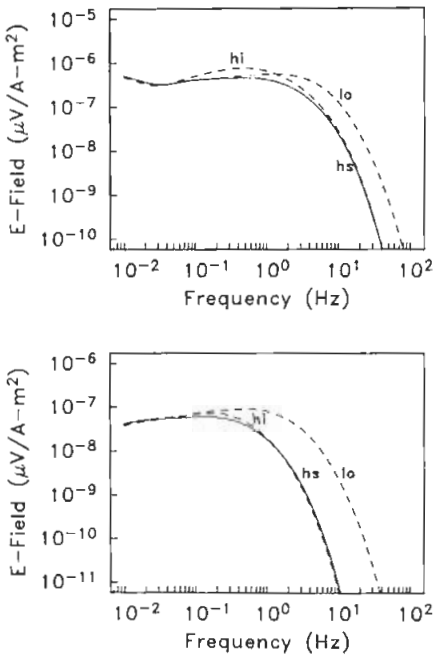

Fig. 17. The radial electric field as a function of frequency at a range of 5 km (bottom panel) and 10 km (top panel) for the shallow models of Figure 6. The notations *lo* and *hi* refer to the relative conductivity of the 1 km thick layer buried at 1 km, while *hs* is the response for a half-space of conductivity 0.05 S/m.

where ρ is the source-receiver separation. This results in quantities whose amplitudes and shapes are independent of range, simplifying the conceptual interpretation. Figure 18 shows this dimensionless response for various values of the conductivity ratio between seawater and rock, and also indicates the true time scale for a system operating on the seafloor with a source-receiver separation of 100 m. The system responses are distinctly different for varying values of the conductivity ratio. Cheesman et al. (1987) also discuss the less common case of a conductive seafloor, and show that the VMD and HMD types are sensitive to its conductivity, while the HED response is markedly attenuated. The VMD system appears to be the most suitable choice if conductive material is being investigated.

A visual impression of outward diffusion of an initial transient in the EM field into a double half-space model as a function of time is shown in Figure 19. The source is a two-dimensional (2-D) electric dipole. Each contour map of the electric current stream function represents a snapshot at the times indicated following a unit increase in the source dipole moment. At the instant the source is activated, two current vortices form, one above and one below the source. The lower layer vortex circulates in the crust and in a narrow band of seawater near the seafloor. The streamlines at large range in the vicinity of the interface strikingly resemble the wavefronts of a seismic head wave. The upper vortex is more compact and confined to the seawater. Clearly, EM energy arrives at a point in the sea just above the seafloor at two distinct times by two different mechanisms. As time progresses, both vortices expand and finally, at the late time limit, the contours match those of a 2-D static dipole, and no current crosses the interface.

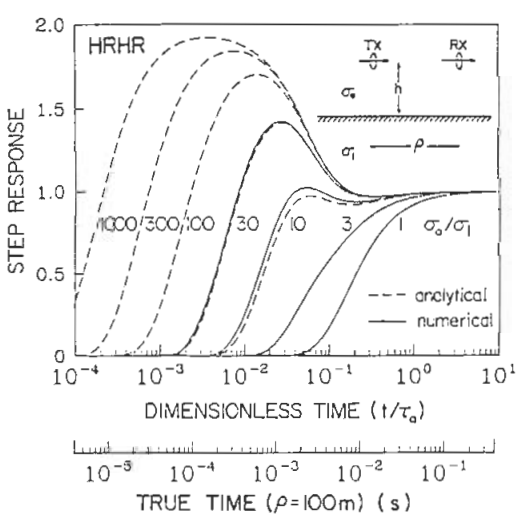

Fig. 18. The normalized step-on response for the coaxial horizontal magnetic dipole-dipole (HMD) system computed analytically (dashed) and numerically (solid) for a range of the ratio of seawater to seafloor conductivity. The magnetic response is normalized by the late-time or dc value, while the time axis is normalized by the diffusion time in seawater (15). A dimensional time axis for a range of 100 m is also shown.

A simplified treatment of both layered earth models and those containing some type of higher dimensional complexity may be obtained for a transient system by recognizing that when the seafloor is more resistive than seawater, the form of the response at early time is dictated principally by the electrical conductivity of the seafloor, and so the ocean may be regarded as a perfect conductor. At later times, the response is determined by the conductivity of seawater, and then the seafloor may be modeled as an insulator. A given response may be approximated by the simple superposition of the early and late time effects. However, as the late time response is nearly independent of the conductivity of the seafloor, the behavior for different crustal models may be compared by examination only of the early time transient.

Cheesman et al. (1987) investigated the coaxial HMD response for models containing a crustal layer over very resistive and highly conductive halfspaces and one containing a thin resistive layer. In each case, the upper ocean half-space is assumed to be perfectly conductive as explained above. The presence of a resistive basement, illustrated in Figure 20, was found to shift the half-space response to earlier time, with the amount of the shift being a strong function of the depth to basement and larger changes corresponding to smaller basement depths. This shift occurs because the resistive basement provides a faster path for the transient signal, yielding earlier arrivals. The shift is minimal for depths to basement exceeding one-half of the transmitter-receiver separation, establishing a rough bound on the depth of investigation. The conductive basement model displays an increased transient amplitude as the thickness of the overlying layer is reduced, with an asymptotic approach to a change by a factor of two. This change occurs because the images of the transmitter current in two very good conductors (the ocean and basement) reinforce the horizontal magnetic field; this effect becomes more intense as the two conductors are closer together, or as basement depth decreases. The arrival time of the transient is not appreciably changed as the depth to basement is altered. The resistive layer displays a much stronger effect on the TEM response than the simpler resistive basement model. In the latter instance, the transient shape is not appreciably changed as basement depth is altered, while the resistive layer model shows marked amplitude and shape variation. For instance, a layer buried at a depth of one tenth of

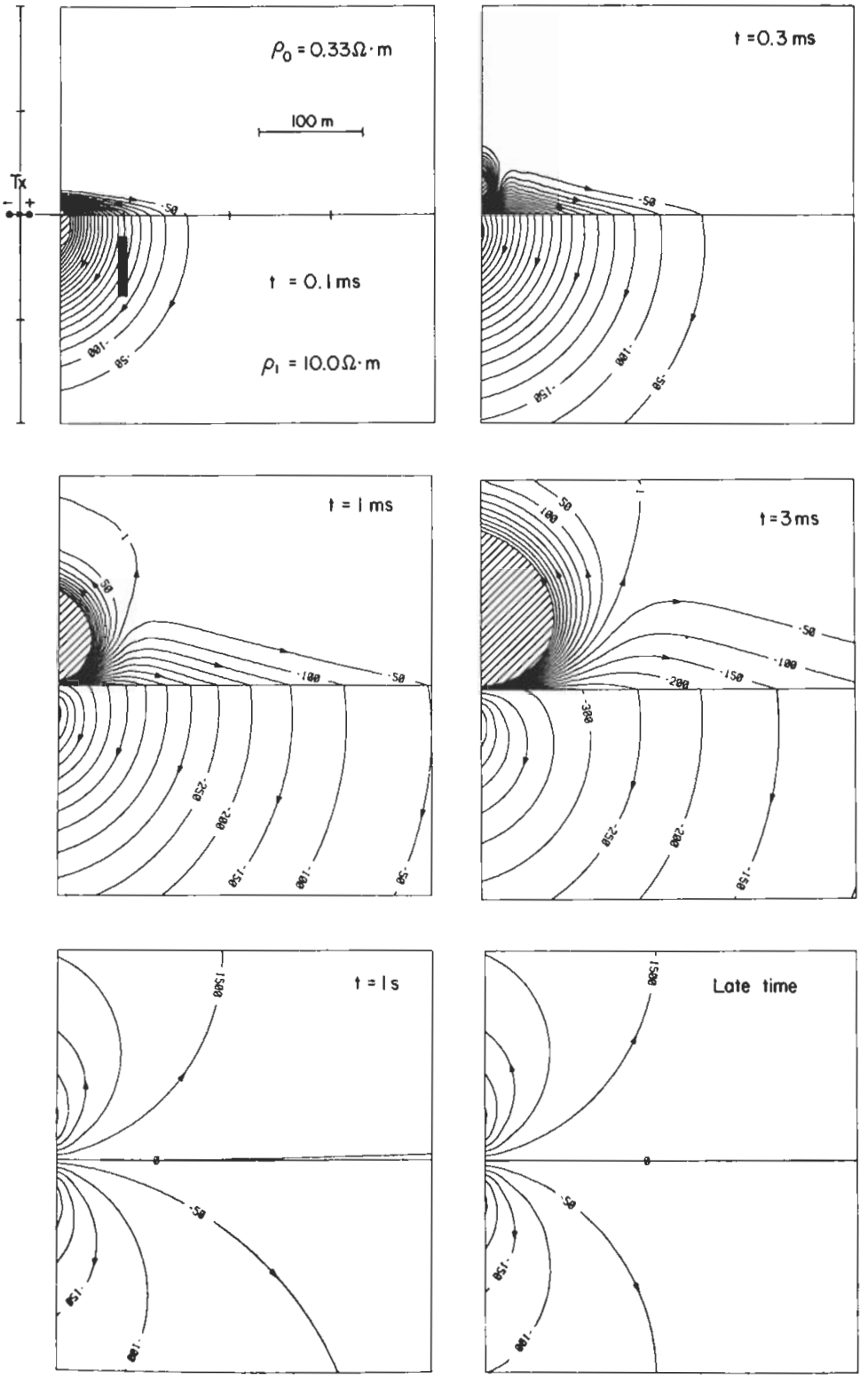

Fig. 19. The outward diffusion of electric current into a double half-space model is shown in the time domain. Each contour map of the current stream function represents a snapshot at the times indicated following a unit increase in the moment of a 2-D electric dipole source. The numbers on the contours have units of mA/km. The amplitude of the current density at a point is the local gradient of the map. The direction of the current density is parallel to the contour. Within the shaded area, the contour lines are too dense to show clearly. The conductivities σ_0 and σ_1 have values of 3 S/m and 0.1 S/m, respectively. Notice that the density of contours in the vicinity of a 2-D target shown in black is much greater at early time than at the late time limit. One can therefore deduce that the size of any anomaly over the target is largest at early times (From Edwards, 1988).

the source-receiver separation shows a transient amplitude of four times the free space value.

Cheesman et al. (1987) also investigated the response of the HMD system to a finite conductive vertical dike. If the dike is positioned between the transmitter and receiver, the response is found to be insensitive to their actual locations, and the dike serves to delay the arrival of the received signal. The incremental delay caused by the dike is linearly related to its conductance. This relation suggests that the time delay can be inverted directly to give some measure of the anomalous integrated conductivity of the seafloor which lies between the source and receiver.

Table 1 is a collection of the most useful formulas for the frequency and transient (step-on) response of two half-spaces in contact for a variety of geometries. In all instances, the variable s may be set to $i\omega$ to get the frequency domain response; the remaining variables are self-explanatory.

Experimental CSEM

A submarine HED system has been proposed and developed at Scripps Institution of Oceanography for deep sounding of the oceanic lithosphere (Cox, 1980, 1981; Chave and Cox, 1982; Young and Cox, 1981; and Cox et al., 1986). This system utilizes a long, insulated seafloor transmitting antenna with bared ends that is energized at frequencies near 1 Hz and a series of horizontal electric field receivers emplaced on the seafloor at ranges of 1–200 km from the source. The HED approach offers several unique advantages for deep electrical conductivity studies. The system is sensitive to both low and high conductivity material in different ways due to the presence of both TM and PM modes, and a horizontal electric source in a high conductivity region (the ocean) couples to a low conductivity region (the seafloor) better than a vertical electric or magnetic source by a factor of the ratio of the conductivities of seawater to rock, which is typically 100 or more.

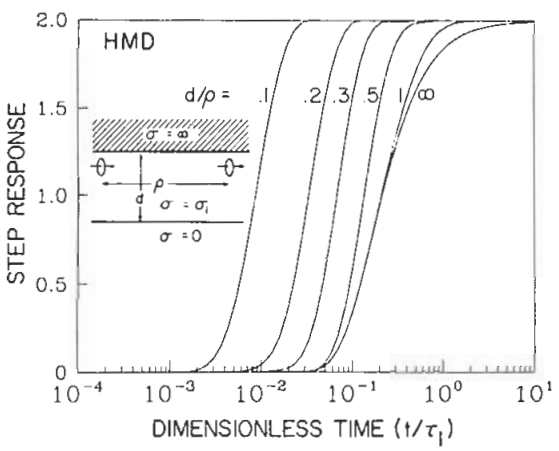

Fig. 20. The step-on response of the double half-space model modified by including a resistive basement at depth d for a range of values of the normalized layer thickness. The ocean has been approximated as a perfect conductor; see text for details.

The seafloor-based transmitter is connected to a surface power source by an insulated cable. The receivers are separate, self-contained, seafloor-based horizontal electric field recorders. This apparatus has been used successfully in the deep ocean on three occasions, with the East Pacific Rise results reported in Spiess et al. (1980) and Young and Cox (1981), and more recent data from the North Pacific collected during 1983 and 1984 covered in Cox et al. (1986).

The transmitter is shown schematically in Figure 21. A surface generator is located either in a moored buoy or on board a research ship and supplies power through an insulated, single conductor cable to an underwater unit. The cable must be strong enough to support the weight of the bottom package and wire during deployment and to withstand the complex, dynamic forces on the buoy and ship during operation; high voltage (≈2000 V) alternating current (≈64 Hz) is used to minimize both ohmic losses and the amount of copper required. A seawater return completes the circuit. Under the direction of a CPU, surface electronics send control signals superimposed on a 20 kHz carrier through the same cable to control the operation of the underwater unit.

The seafloor instrument package transforms the high voltage ac to a lower voltage (≈100 V) and detects the control signal for use by a local processor. The electronics switch a set of silicon controlled rectifiers connected as a full wave bridge to synthesize waveforms in the range 1/16–16 Hz with nearly equal first and third harmonics and minimal power at other frequencies. The transmitting dipole antenna is a 500–1000 m insulated cable terminated in stainless steel electrodes 15 m long, has an intrinsic resistance of about 1 Ω, and has a small resistance with respect to seawater. This antenna yields a source current of about 100 A from a generator of 15–30 kW capacity.

The electric field receivers utilize Ag-AgCl electrodes to couple to seawater and act as recording voltmeters, similar to the operation of seafloor MT instrumentation. There are two basic types of electric field recorders in use: the first is a free-fall type which uses a pair of rigid, orthogonal antennae of 9 m span, while the second measures the potential between the ends of a 200–3000 m long, insulated, copper wire. The first type is called an ELF (Electric Field recorder) and was the only receiver used in the 1979 RISE experiment (Young and Cox, 1981). The fixed pair of receiving dipoles forms part of the heavy anchor assembly.

Table 1. The frequency and transient step-on EM responses of two half-spaces in contact.

The Coaxial Magnetic Dipole-Dipole

$$H_\rho(s) = \frac{I\Delta A}{2\pi\rho^3(\tau_0 - \tau_1)s} \times \left\{ -\sqrt{\tau_0 s(\tau_1 s)^3}K_1(\sqrt{\tau_1 s}) - [\sqrt{\tau_0 s}(\tau_1 - \tau_0)s + (2\tau_1 - 5\tau_0)s - 12\sqrt{\tau_0 s} - 12]\exp(-\sqrt{\tau_0 s}) + [\sqrt{\tau_1 s}(2\tau_0 - \tau_1)s + (2\tau_0 - 5\tau_1)s - 12\sqrt{\tau_1 s} - 12]\exp(-\sqrt{\tau_1 s}) \right\},$$

$$H_\rho^s(t) = \frac{I\Delta A}{2\pi\rho^3(\tau_0 - \tau_1)} \left[-\tau_1\sqrt{\frac{\tau_0}{t}}\exp\left(-\frac{\tau_1}{8t}\right)W_{1/2,1/2}\left(\frac{\tau_1}{4t}\right) + (\tau_0 - \tau_1 + 12t)\sqrt{\frac{\tau_0}{\pi t}}\exp\left(-\frac{\tau_0}{4t}\right) - (\tau_0 + 2\tau_1 - 12t)\,\mathrm{erfc}\left(\sqrt{\frac{\tau_0}{4t}}\right) + (2\tau_0 - \tau_1 - 12t)\sqrt{\frac{\tau_1}{\pi t}}\exp\left(-\frac{\tau_1}{4t}\right) + (2\tau_0 + \tau_1 - 12t)\,\mathrm{erfc}\left(\sqrt{\frac{\tau_1}{4t}}\right) \right].$$

The Vertical Coplanar Magnetic Dipole-Dipole

$$H_z(s) = \frac{I\Delta A}{2\pi\rho^3(\tau_0 - \tau_1)s}\{[9 + 9\sqrt{\tau_0 s} + 4\tau_0 s + (\sqrt{\tau_0 s})^3]\exp(-\sqrt{\tau_0 s}) - [9 + 9\sqrt{\tau_1 s} + 4\tau_1 s + (\sqrt{\tau_1 s})^3]\exp(-\sqrt{\tau_1 s})\}.$$

$$H_z^s(t) = \frac{9I\Delta A}{2\pi\rho^3}\frac{t}{\tau_0 - \tau_1}\left[\left(1 - \frac{\tau_0}{18t}\right)\mathrm{erfc}\left(\sqrt{\frac{\tau_0}{4t}}\right) + \sqrt{\frac{\tau_0}{\pi t}}\left(1 + \frac{\tau_0}{9t}\right)\exp\left(-\frac{\tau_0}{4t}\right) - \left(1 - \frac{\tau_1}{18t}\right)\mathrm{erfc}\left(\sqrt{\frac{\tau_1}{4t}}\right) - \sqrt{\frac{\tau_1}{\pi t}} \times \left(1 + \frac{\tau_1}{9t}\right)\exp\left(-\frac{\tau_1}{4t}\right).$$

The Vertical Magnetic Field of an Electric Dipole

$$H_z(s) = \frac{I\Delta l}{2\pi\rho^4 s}\frac{1}{\sigma_0 - \sigma_1}[(3 + 3\sqrt{\tau_1 s} + \tau_1 s)\exp(-\sqrt{\tau_1 s}) - (3 + 3\sqrt{\tau_0 s} + \tau_0 s)\exp(-\sqrt{\tau_0 s})].$$

$$H_z^s(t) = \frac{3\mu_0 I\Delta l}{2\pi\rho^2}\frac{t}{(\tau_0 - \tau_1)}\left[\left(1 - \frac{\tau_1}{6t}\right)\mathrm{erfc}\left(\sqrt{\frac{\tau_1}{4t}}\right) + \sqrt{\frac{\tau_1}{\pi t}}\exp\left(-\frac{\tau_1}{4t}\right) - \left(1 - \frac{\tau_0}{6t}\right)\mathrm{erfc}\left(\sqrt{\frac{\tau_0}{4t}}\right) - \sqrt{\frac{\tau_0}{\pi t}}\exp\left(-\frac{\tau_0}{4t}\right)\right].$$

The Vertical Magnetic Field at the Center of a Finite Loop

$$H_z(s) = \frac{I}{a(\tau_0 - \tau_1)}[(\tau_1 s + 3\sqrt{\tau_1 s} + 3)\exp(-\sqrt{\tau_1 s}) - (\tau_0 s + 3\sqrt{\tau_0 s} + 3)\exp(-\sqrt{\tau_0 s})]$$

where the time constant is defined as

$$\tau_i = \mu_0\sigma_i a^2.$$

$$H_z^s(t) = \frac{3I}{a}\frac{t}{(\tau_0 - \tau_1)}\left[\left(1 - \frac{\tau_1}{6t}\right)\mathrm{erfc}\left(\sqrt{\frac{\tau_1}{4t}}\right) + \sqrt{\frac{\tau_1}{\pi t}}\exp\left(-\frac{\tau_1}{4t}\right) - \left(1 - \frac{\tau_0}{6t}\right)\mathrm{erfc}\left(\sqrt{\frac{\tau_0}{4t}}\right) - \sqrt{\frac{\tau_0}{\pi t}}\exp\left(-\frac{\tau_0}{4t}\right)\right].$$

The Horizontal Coaxial Electric Dipole-Dipole

$$E_\rho(s) = \frac{I\Delta l}{2\pi\sigma_0\rho^3}\left\{(1 + \sqrt{\tau_0 s})\exp(-\sqrt{\tau_0 s}) + (1 + \sqrt{\tau_1 s} + \tau_1 s)\exp(-\sqrt{\tau_1 s}) - \sqrt{\frac{\sigma_1}{\sigma_0}}\left[\tau_1 s K_1(\sqrt{\tau_1 s}) + (\sqrt{\tau_1 s})^3 K_0(\sqrt{\tau_1 s})\right]\right\}.$$

$$E_\rho^s(t) = \frac{I\Delta l}{4\pi\sigma_0\rho^3}\left\{\mathrm{erfc}\left(\sqrt{\frac{\tau_0}{4t}}\right) + \sqrt{\frac{\tau_0}{\pi t}}\exp\left(-\frac{\tau_0}{4t}\right) + \mathrm{erfc}\left(\sqrt{\frac{\tau_1}{4t}}\right) + \sqrt{\frac{\tau_1}{\pi t}}\left(1 + \frac{\tau_1}{2t}\right)\exp\left(-\frac{\tau_1}{4t}\right) + \frac{\sigma_1}{\sigma_0}\sqrt{\frac{\tau_0}{t}}\exp\left(-\frac{\tau_1}{8t}\right) \times \left[\left(1 - \frac{\tau_1}{2t}\right)W_{1/2,1/2}\left(\frac{\tau_1}{4t}\right) - \frac{\tau_1}{4t\sqrt{\pi}}K_1\left(\frac{\tau_1}{8t}\right)\right]\right\}.$$

Table 1. Continued.

The Horizontal Magnetic Field of a Vertical Magnetic Dipole

$$H_\rho(s) = \frac{I\Delta A}{4\pi\rho^3}(\tau_0 - \tau_1)s\left[I_2(a\sqrt{s})K_2(b\sqrt{s}) - \frac{\alpha+1}{\alpha-1}I_1(a\sqrt{s})K_1(b\sqrt{s})\right],$$

where

$$a = \frac{\sqrt{\tau_0} - \sqrt{\tau_1}}{2},$$

and

$$b = \frac{\sqrt{\tau_0} + \sqrt{\tau_1}}{2},$$

$$H_\rho^s(t) = \frac{I\Delta A}{4\pi\rho^3}\frac{(\tau_0 - \tau_1)}{2t}\exp\left(-\frac{\tau_0+\tau_1}{8t}\right)\left[I_2\left(\frac{\tau_0-\tau_1}{8t}\right) - \frac{\alpha+1}{\alpha-1}I_1\left(\frac{\tau_0-\tau_1}{8t}\right)\right].$$

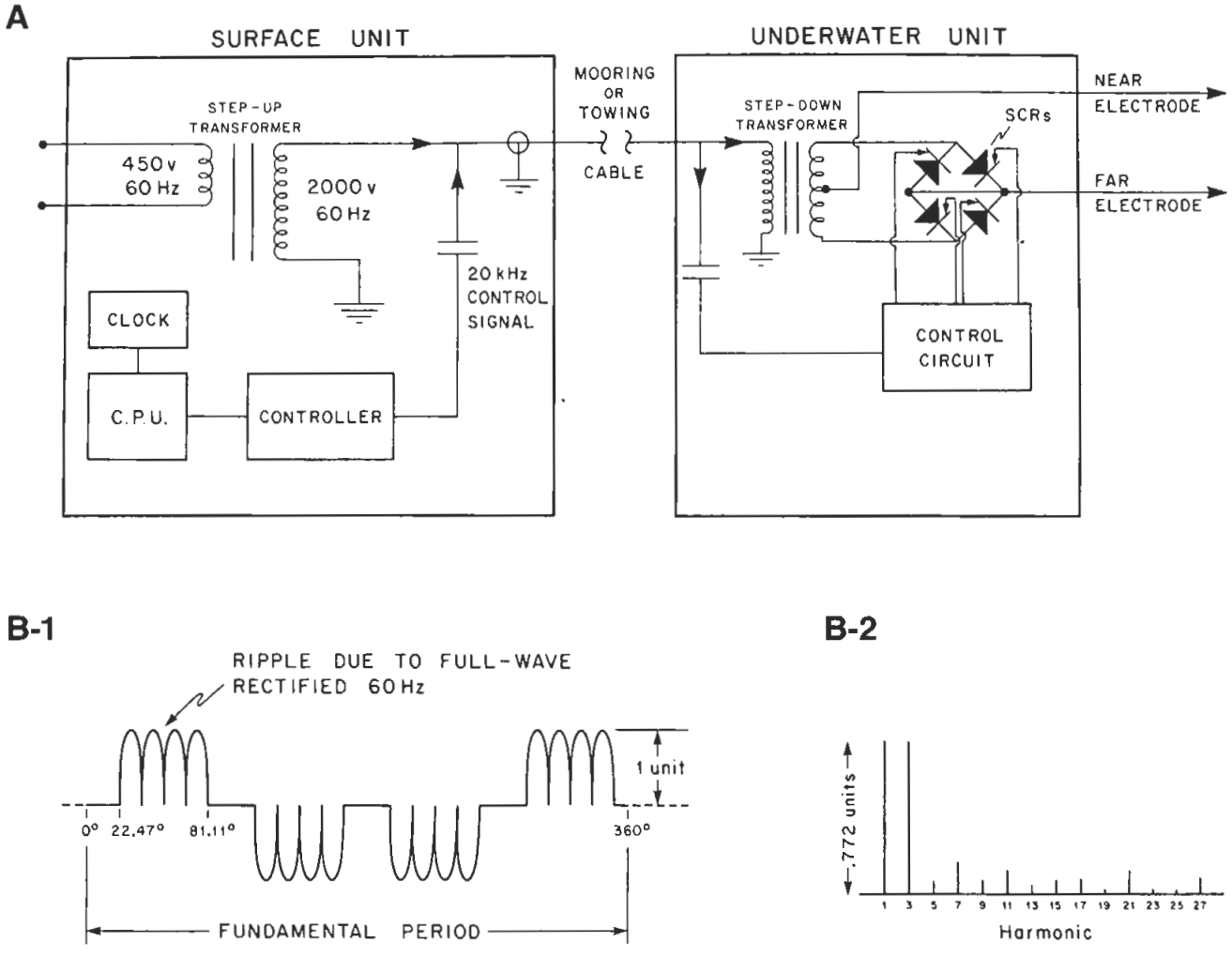

Fig. 21. Schematic of the HED transmitter design used at Scripps Institution of Oceanography (A). The lower panel (B-1) shows the transmitted waveform, obtained by switching the source half cycles. The phase of the switching is chosen to maximize the power at the fundamental and third harmonic (B-2).

The Ag-AgCl electrodes are fixed to the ends of the antenna arms and weighted to hold them as close as possible to the seabed, minimizing noise from water motion. Special low-noise amplifiers are used to increase the signal level for internal processing and recording.

Much of the measurement noise is generated by the electrodes, and greater sensitivity may be achieved by substantially increasing the antenna length. The second type of instrument, called a LEM for Long antenna EM recorder, has an antenna consisting of 200–3000 m of 6AWG insulated copper wire terminated by large (0.5 m) Ag-AgCl electrodes, and is described in Webb et al. (1985). The unit is deployed dynamically by streaming the antenna behind the ship and then lowering the instrument on a winch with enough way on the ship to maintain a straight antenna (typically, 1–3 knots); the system is then released within a few meters of the seafloor. These instruments were used to accomplish the longer source-receiver spacings used in the 1983 and 1984 experiments (Cox et al., 1986). Figure 22 shows a LEM instrument in its launching cradle.

Common features of the ELF and LEM units include the use of special, low noise, low impedance Ag-AgCl electrodes which differ from the usual MT design by being much larger (Webb et al., 1985), and the application of acoustic techniques to allow location and (for the LEM's) orientation on the seafloor to be determined from the surface ship. Data are collected on digital magnetic tape under the control of a CPU; this CPU allows the use of synchronous stacking and block averaging techniques to reduce the necessary tape capacity.

Figure 23 shows the layout for an ideal experiment. The ELF instruments are placed 5–20 km from the transmitter, while the LEM units are deployed up to 100 km or more away. The transmitter is then lowered to the seafloor and either connected to a surface buoy if a moored configuration is used or towed slowly (0.5–2 knots) behind a surface ship. A potential problem associated with towing the transmitter is that the

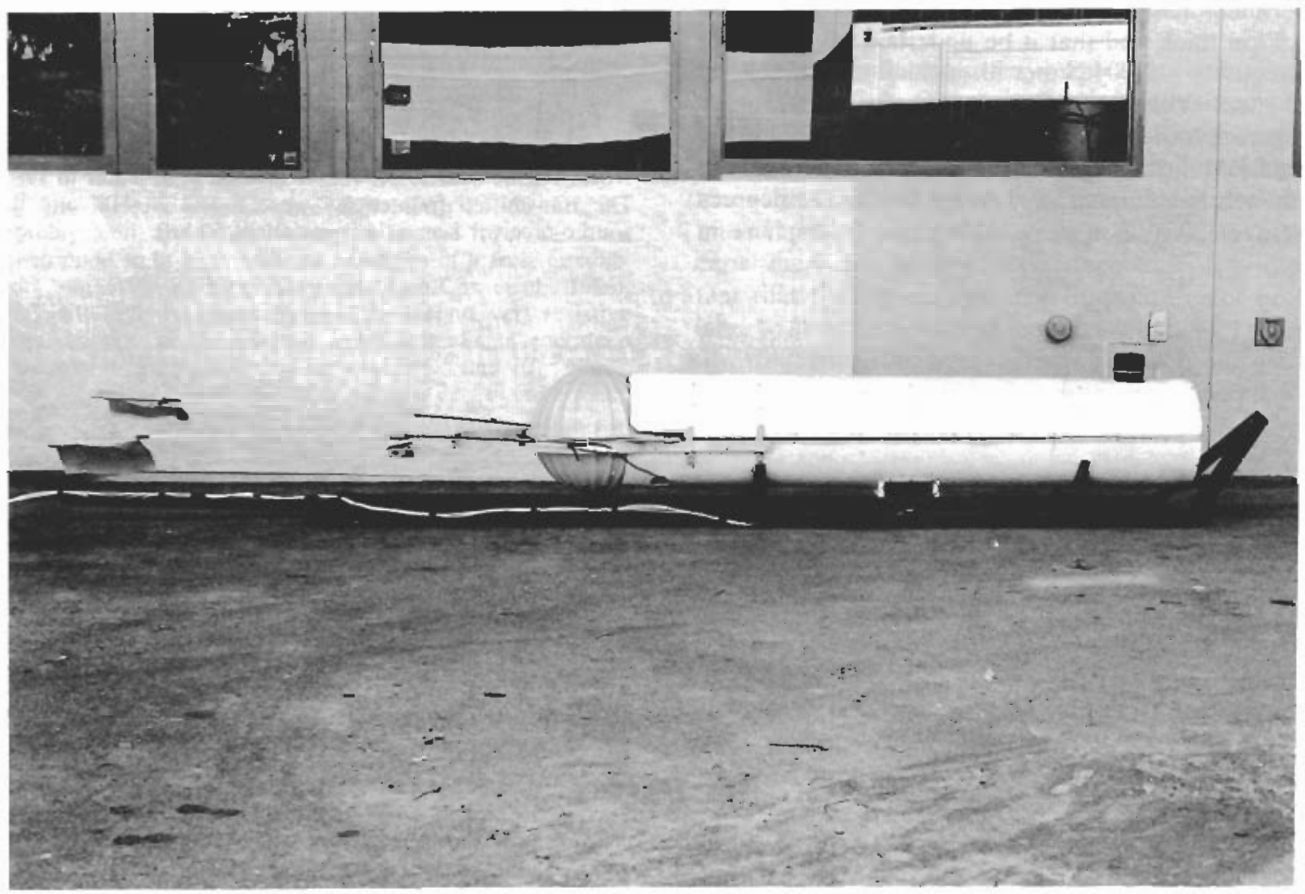

Fig. 22. Photograph of a LEM instrument in its launching cradle. The aluminum pressure case is contained in a protective plastic tube containing glass ball flotation, radio beacons, and light strobes to aid in locating the package after release. The instrument sits on a steel sled which is dropped under internal timer control at recovery time. The receiving antenna is attached at the right end of the unit.

phase coherence necessary for stacking techniques to operate correctly may be lost at high frequencies where the wavelength (i.e., the skin depth) is small, although there was no indication of this at the greatest frequency (24 Hz) used in the 1983 and 1984 experiments. A preprogrammed set of transmitting frequencies, synchronized with the receiver stacking algorithm in the seafloor instruments, is then run for a period of several days. This run is followed by recovery of all instruments.

The RISE experiment (Spiess et al., 1980) yielded the first results from the HED method. An ELF receiver was placed 19 km from a ship-towed transmitter and data were collected in the frequency range 0.25–2.25 Hz. A signal-to-noise (S/N) ratio of better than 5 was achieved at all frequencies by stacking the data to an equivalent bandwidth of 1 cycle per hour. There is essentially no high conductivity sediment cover on mid-ocean ridges, and the uppermost basalt layer of the oceanic crust is predicted to have a conductivity of ≈0.05 S/m to a depth of at least 1 km from the results of the downhole resistivity experiment (e.g., Becker et al., 1982). The results of the RISE experiment require that this layer be no more than 1–1.5 km thick and that it be underlain by a layer of conductivity <0.004 S/m with a thickness of several kilometers (Young and Cox, 1981).

Figure 24 shows a typical measurement collected using LEM instruments during the 1984 experiment in the North Pacific near 29 degrees north, 122 degrees west over 20 million year old oceanic lithosphere in 4300 m of water. There is only limited (<30 m) sediment cover in this area, so that attenuation of the fields by the surface layer is negligible. The transmitted frequencies in this example were 8 and 24 Hz. Data were collected during this experiment over ranges of

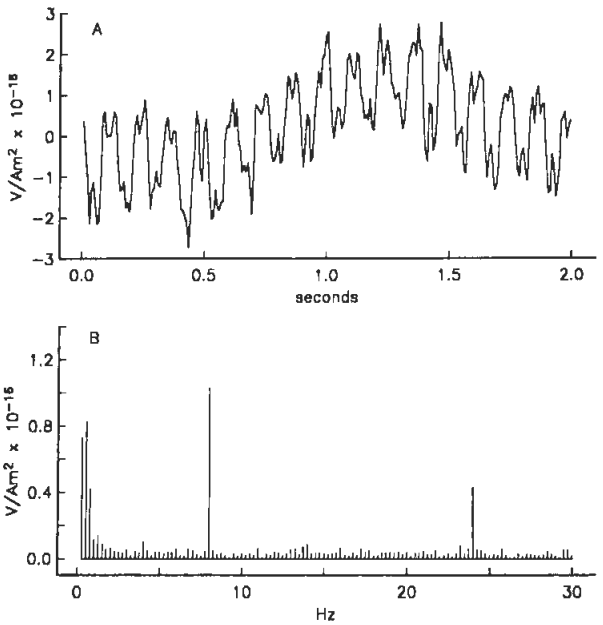

Fig. 24. Typical data collected by a LEM instrument in the North Pacific near 29°N, 122°W in 4300 m of water in 1984. The transmitted frequencies were 8 and 24 Hz, and the source-receiver separation was about 60 km.

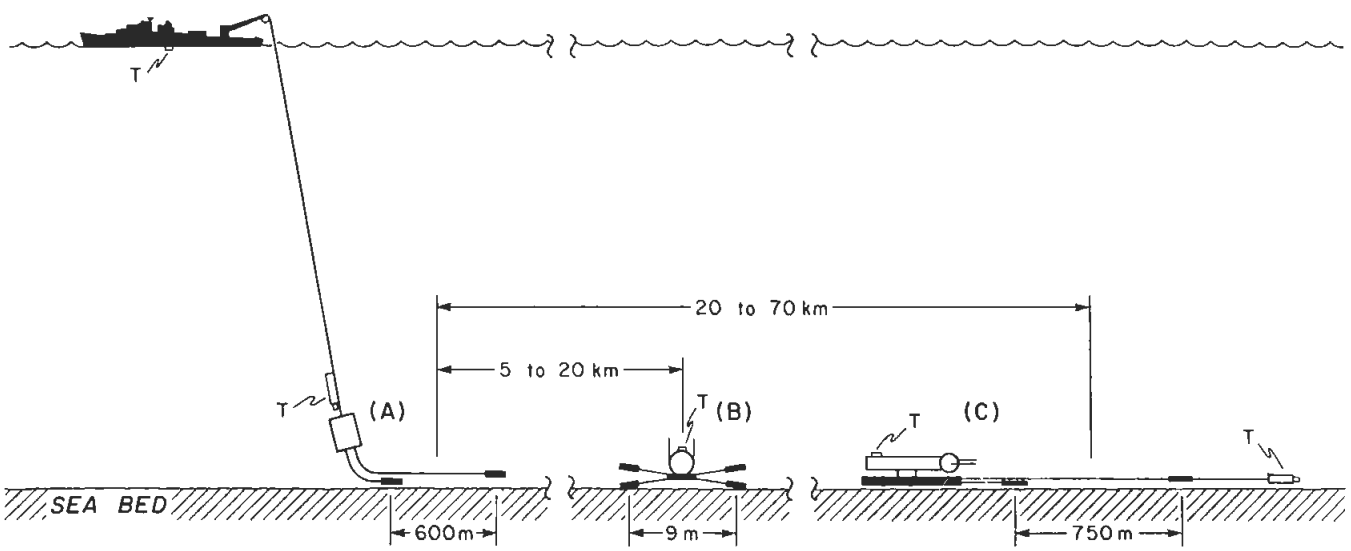

Fig. 23. Typical layout for an HED deep sounding experiment. A surface ship or buoy supplies power to the seafloor transmitter (A) through a single conductor cable with a seawater return. The transmitter switches the input waveform to synthesize the signal shown in Figure 21 and drives an insulated antenna (with bared ends) of about 600 m length. Either ELF (B) or LEM (C) receivers are placed at ranges of 5 to 70 km or more from the transmitter. Acoustic transponders (T) are used to locate all of the seafloor components from a surface ship.

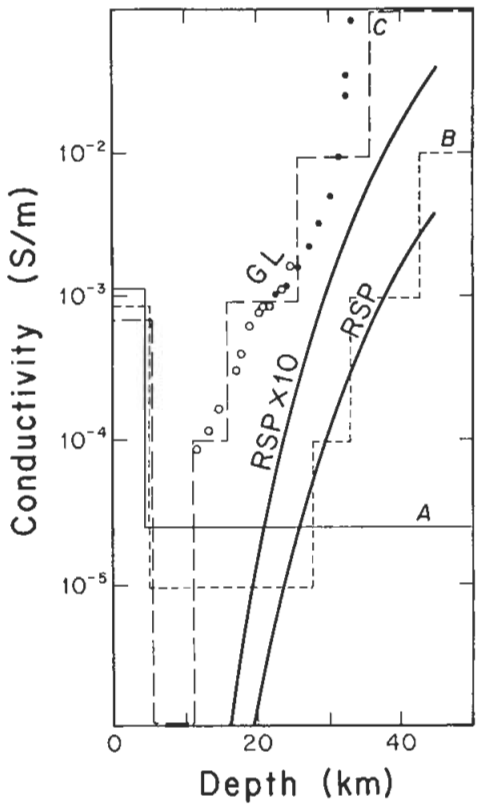

Fig. 25. Models which fit the 1984 North Pacific data acceptably well. Structure below the second layer has been constrained to fit high and low extremes of mantle conductivity suggested by laboratory data (see Cox et al., 1986). Thus, although the conductivity of the second, very resistive layer, cannot be determined independently of the deep structure, it can be bounded between 10^{-6} and 10^{-5} S/m.

20–70 km and frequencies of 0.06–24 Hz, and an interpretation is reported in Cox et al. (1986). Figure 25 shows some simple models which fit these data. The results indicate that an extremely resistive upper mantle, with a conductivity of about 10^{-5} S/m, underlies a 5 km thick crust of conductivity $\approx 10^{-3}$ S/m. The thickness of the resistive mantle region is not well-determined, but laboratory data for olivine conductivity (Duba et al., 1974) may be used to limit it to a maximum depth of 30 km. Cox et al. (1986) inferred an upper limit of about 0.1 percent by volume for free water in the uppermost mantle based on these data.

The controlled source group at Scripps has also developed and tested a system for EM surveying on the continental shelf. Figure 26 shows the layout of this towed system. The layout is based on the same frequency domain dipole-dipole system used for deep sounding, so the theory developed by Chave and Cox (1982) and Chave (1984b) is directly applicable. In particular, it may be shown that resistive features such as permafrost layers and basalt flows can be mapped using frequencies and source-receiver ranges attainable by the experimental system (Constable et al., 1986).

The receiver for the survey array is towed in tandem with the transmitter at the end of a floating rope which may be winched in or out to vary the source-receiver spacing. The receiver records the data internally on magnetic tape, but a sample of the data is also transmitted to the surface ship over a radio link so that the experiment may be monitored in real time. It is important that the power from the transmitter not be too large to avoid overloading the receiver at short ranges, low frequencies, or over resistive seafloor, and careful oversight of this parameter is necessary. The receiver

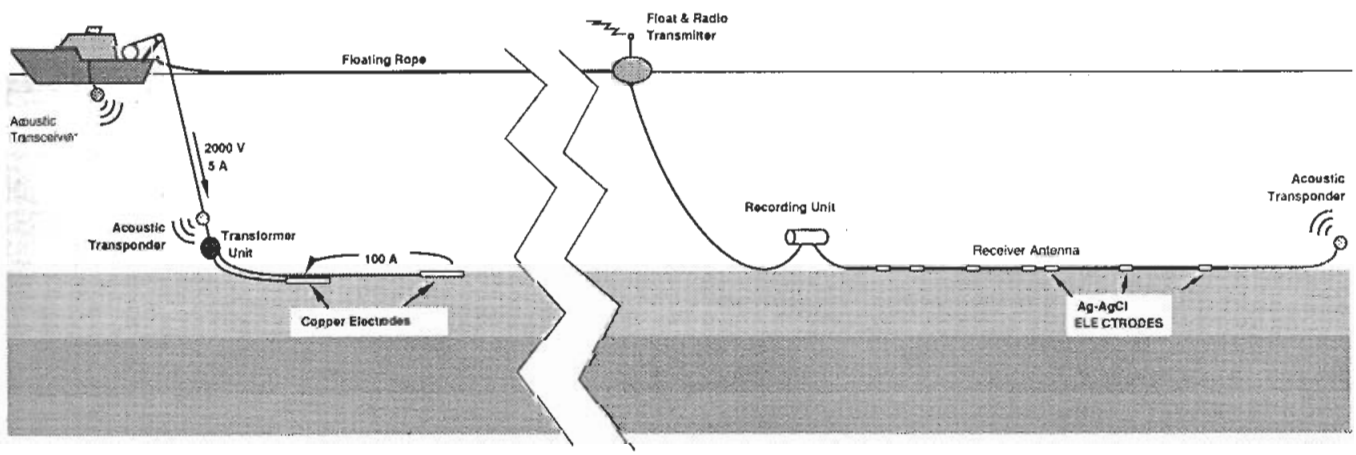

Fig. 26. Sketch showing the towed frequency-domain profiling system developed at Scripps Institution of Oceanography. The source antenna is towed immediately behind a research ship and powered by the ship's generators. The receiving antenna is towed farther aft from a radio-equipped float and consists of an array of Ag-AgCl electrodes with acoustic transponders for location.

antenna must be dragged in contact with the seabed and so must withstand a high degree of abuse, but by maintaining a smooth and streamlined antenna surface problems seem to be obviated.

The operation of the transmitter is much like that of the deep sea unit except that the shorter towing cable and higher frequency of operation allow the transmitted waveform to be generated on board ship rather than synthesized in the submerged electronic package. Thus, high voltage and low current at the appropriate frequency is sent via the towing cable to the underwater unit where it is simply transformed to lower voltage, making about 100 A available for the 50 m transmitter antenna. The transmitter electrodes are 7 m lengths of copper tube about 7 cm in diameter. The entire operation is monitored and navigated by means of acoustic transponders attached to the transmitter, recording unit, and receiver antenna.

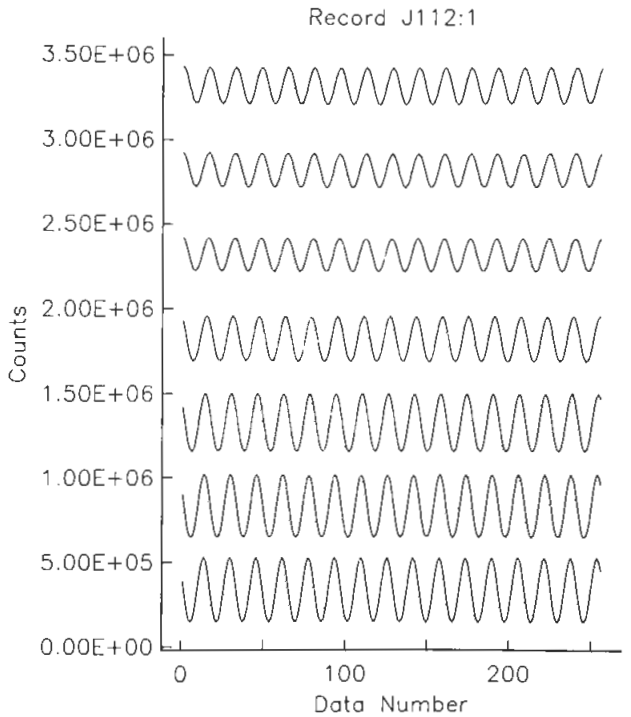

Fig. 27. The received signal in instrument counts for the towed frequency-domain system at 7 points spaced about 100 m apart. The transmitted frequency is 64 Hz. See text for details.

An initial test off of San Diego demonstrates the feasibility of the technique. Figure 27 shows the received signal at 7 consecutive locations spaced about 100 m apart. The transmitted frequency is 64 Hz and the source-receiver spacing is 500 m. The excellent S/N ratio is clear from inspection of the records. The signals are up to 6 V peak-to-peak after amplification and stacking, corresponding to responses of 3 to 6 $\times$ 10^{-11} V/A-m^2 or a 1 to 0.8 Ω·m half-space resistivity. As the seafloor resistivity decreases, the amplitude of the signal decays and the phase advances. Further work with this towed survey system is planned.

Experimental CSEM—Time Domain

The prototype of a time-domain HMD system, shown in Figure 28, has been constructed and tested at the University of Toronto (Cheesman et al., 1988). The magnetic dipole transmitter consists of a fiberglass cylinder, 2 m long and 1 m in diameter, in which 100 turns of wire are embedded and evenly spaced along its length. The cylinder is open ended and has three internal radial fins running its entire length for strength and hydrodynamic streamlining. The front end is tapered slightly to prevent scooping of bottom sediments from occurring as it is dragged forward. Current to the

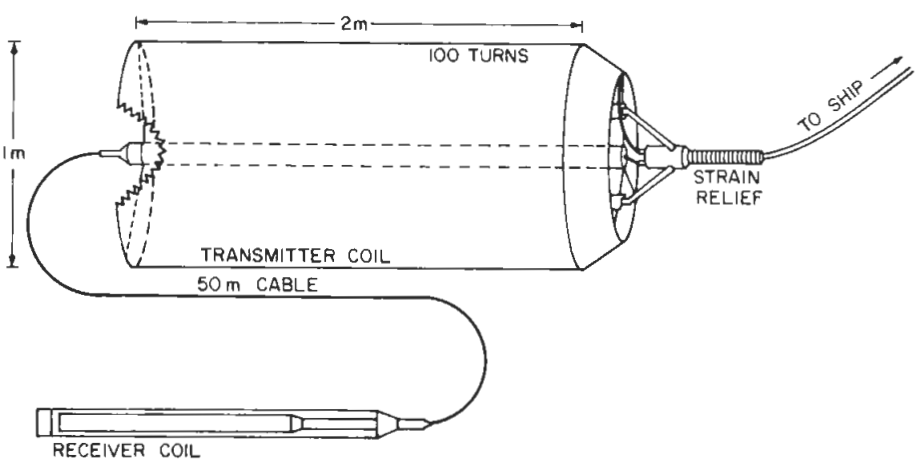

Fig. 28. Sketch of the HMD transmitter design used at the University of Toronto. A transmitter coil containing 100 turns of wire is connected to a surface ship by an electric cable. The receiver, a coil wound on an iron core, is streamed behind the transmitter and encased in a protective plastic sleeve.

transmitter coil is supplied by a transmitter and transformer on the ship which is powered by a pair of automotive batteries. The polarity of the current is reversed every 5 ms to provide the EM transient.

A modified iron-core coil serves as the receiver. The coil is enclosed in a protective polycarbonate tube, and is joined to the transmitter by a 50 m cable. The entire array is towed along the seafloor by a heavy wire spooled on a winch so that its length may be varied with the water depth. Unshielded conductors within the wire carry both the transmitted current and the received voltage signal. An analog delay line installed in the receiver retards the returned signal by 2 ms, a point well after the main effect of the transmitter voltage transient. The cost-effective solution eliminates the need for a specially constructed cable containing either shielded wires or fiber optics.

A test survey was performed in the Trincomali Channel near the southeast end of Vancouver Island at about 48° 55′N, 123° 27′W (see Figure 29) where the water depth ranges from 30 to 100 m. The seafloor consists of bedrock overlain by varying thicknesses of mud, ranging from zero to tens of meters, so that the response of the system to varying thicknesses of sediment could be ascertained. A total of 38 measurements were made at 19 sites along 3 lines.

The signal was digitally sampled at 100 kHz. Each 10.24 ms signal record consisted of 1024 samples, and was triggered directly from the transmitter. An average signal waveform was produced by stacking 512 signals. The acquisition of an averaged signal took about 90 s. Signal amplitudes ranged from 30 to 160 mV, with a background noise of about 1 mV in the stacked signals. The averaged signal waveforms were stored digitally on floppy disks. It is necessary to keep the receiver stationary while measurements are being made to avoid motional emfs induced in the coil. However, it was possible for the ship to maintain a constant way by paying out the tow cable whenever a measurement was made and then reeling it in between sites.

Interpretation of the data began with the production of a set of theoretical type curves. The model chosen is a double half-space, representing seawater over a homogeneous conductor. Figure 30 shows the tran-

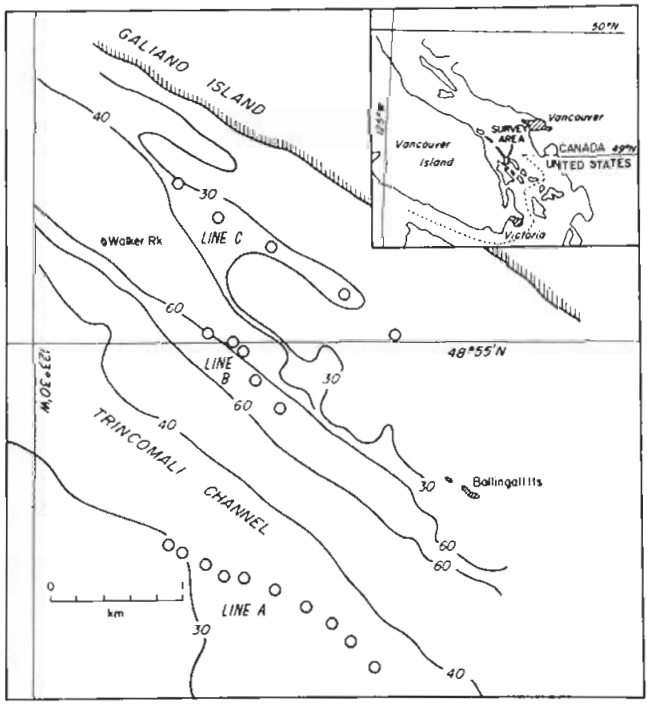

Fig. 29. Location map showing the site of a test of the HMD time-domain apparatus. Measurements were made along three lines, at positions indicated by the open circles. The water depth contours are in meters.

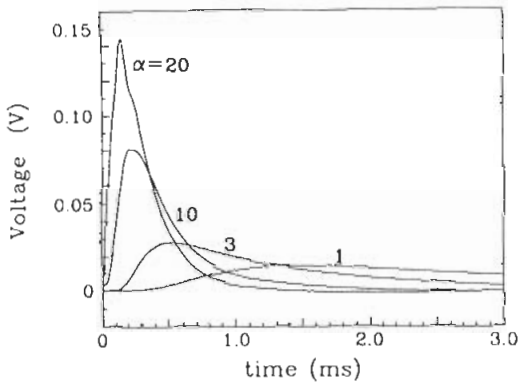

Fig. 30. Theoretical signals for selected values of the seafloor-to-seawater resistivity contrast α, synthesized by convolving the impulse response of the model with the actual transmitted current and the receiver coil transfer function. Note that both the shape and the amplitude of the transient are diagnostic of the seafloor resistivity.

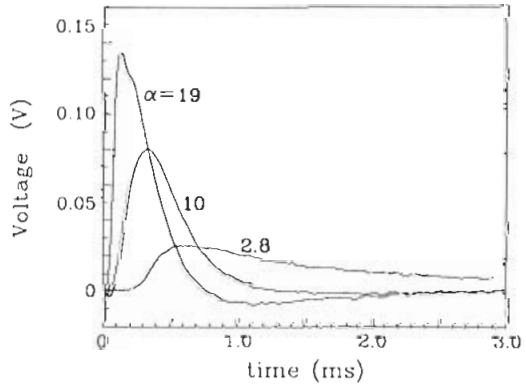

Fig. 31. Actual measured signals from selected sites with interpreted values of the resistivity contrast. These should be compared to the Figure 30 theoretical responses.

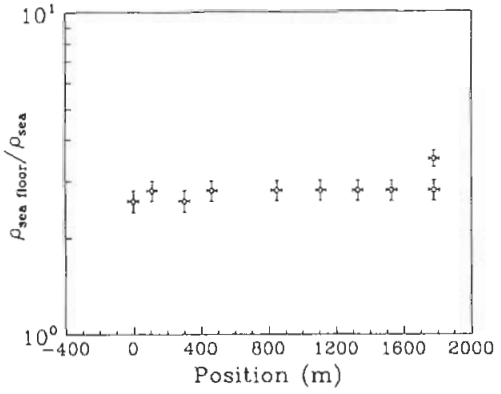

Fig. 32. Interpreted values of the resistivity contrast on Line A. This line covered a relatively featureless area of thick mud which is reflected in the constant seafloor resistivity.

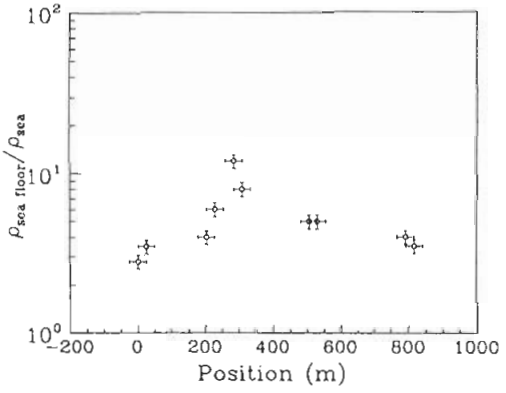

Fig. 33. Interpreted values of the resistivity contrast on Line B. This line crossed an area with minimal seafloor mud, and the maximum in seafloor resistivity corresponds to the thinnest sediments.

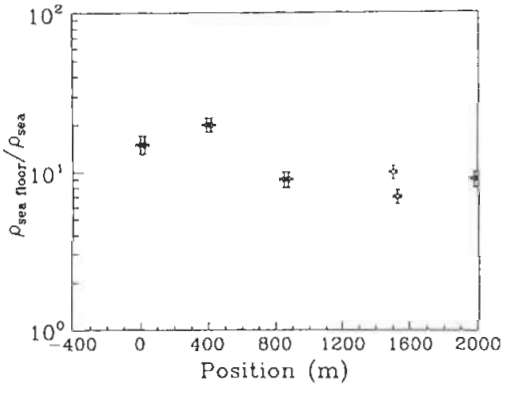

Fig. 34. Interpreted values of the resistivity contrast on Line C. This area had almost no sediment cover, so the seafloor resistivities largely reflect that of the basement rocks.

sient response of the system for models in which the resistivity contrast is 1, 3, 10 and 20. The output of a coil is proportional to the time rate of change of the magnetic field. A relatively resistive seafloor produces a shorter and stronger signal than a more conductive seafloor because of the differences in the rates of diffusion. Thus, both the signal shape and amplitude are indicative of the seafloor resistivity. By matching the delay time and amplitude of an actual signal to the theoretical curves, a value of the resistivity contrast at that site may be determined. Figure 31 shows three of the recorded signals along with the interpreted values for the seafloor resistivity.

The results were also compared with other data. A 3.5 kHz acoustic recorder measured the bottom topography and indicated the presence of thin sediment cover. Line A (Figure 29) traversed a relatively flat, acoustically featureless area of thick mud. The resistivity contrast showed little variation; values of the ratio of seafloor-to-seawater resistivity α ranged between 2.5 and 3.0 (Figure 32). Line B was chosen because it crossed an area where the acoustic recorder indicated that the underlying rock was covered by only 10–25 m of mud. Interpreted resistivities directly correlate with the thickness of the relatively less resistive mud, with values of α varying from 3 where the mud was 25 m or more thick, up to 12 where the mud was about 10 m thick (Figure 33). Line C showed the highest contrasts, with values of α as high as 20 in a region where the acoustic measurements show no covering layer of sediment (Figure 34). All of the measurements are consistent with a model in which a varying thickness of 10 Ω·m mud overlies rock with a resistivity of about 60 Ω·m.

ACKNOWLEDGMENTS

The authors thank K. Becker for information on the downhole resistivity experiments and C. S. Cox, J. H. Filloux, and S. C. Webb for valuable discussions on many aspects of seafloor EM. EM research at Scripps Institution of Oceanography is supported by the Office of Naval Research and the National Science Foundation, while work at the University of Toronto is funded by the Natural Sciences and Engineering Research Council of Canada.

REFERENCES

Armi, L. and D'Asaro, E., 1980, Flow structures of the benthic ocean: J. Geophys. Res., **85**, 469–484.

Backus, G. E., 1986, Poloidal and toroidal fields in geomagnetic field modeling: Rev. Geophys., **24**, 75–109.

Ballard, R. D., Francheteau, J., Juteau T., Rangan, C., and Normark, W., 1981, East Pacific Rise at 21° N: The volcanic, tectonic, and hydrothermal processes of the central axis: Earth Pl. Sci. Lett., **55**, 1–10.

Bannister, P. R., 1968a, Electromagnetic fields within a

stratified earth produced by a long horizontal line source: Radio Science, **3**, 387–390.
———1968b, Determination of the electrical conductivity of the seabed in shallow waters: Geophysics, **33**, 995–1003.
Becker, K., 1985, Large scale electrical resistivity and bulk porosity of the oceanic crust, Hole 504B, Costa Rica Rift: *in* Anderson, R. N., et al., Initial Reports of the Deep Sea Drilling Project, **83**, Washington D.C.: US Government Printing Office, 419–427.
———1990, Large scale electrical resistivity and bulk porosity of the upper oceanic crust at Hole 395A: Proc. ODP, Scientific Results, **109**, Washington, D.C.: US Government Printing Office, 205–212.
Becker, K., Von Herzen, R. P., Francis, T. J. G., Anderson, R. N., Honnorez, J., Adamson, A. C., Alt, J. C., Emmerman, R., Kempton, P. D., Kinoshita, H., Laverne, C., Mottl, M. J., and Newmark, R. L., 1982, In situ electrical resistivity and bulk porosity of the oceanic crust, Costa Rica Rift: Nature, **300**, 594–598.
Brewitt-Taylor, C. R., 1975, Self-potential prospecting in the deep oceans: Geology, **3**, 541–543.
Brimhall, G. H., 1987, Metallogenesis: Rev. Geophys., **25**, 1079–1088.
Butterworth, S., 1924, The distribution of the magnetic field and return current around a submarine cable carrying alternating current—part II: Phil. Trans. Roy. Soc. (Lon.), **A224**, 141–184.
Chave, A. D., 1984a, On the electromagnetic fields induced by oceanic internal waves: J. Geophys. Res., **89**, 10519–10528.
———1984b, The Fréchet derivatives of electromagnetic induction: J. Geophys. Res., **89**, 3373–3380.
Chave, A. D., and Cox, C. S., 1982, Controlled electromagnetic sources for measuring electrical conductivity beneath the oceans, 1., Forward problem and model study: J. Geophys. Res., **87**, 5327–5338.
———1983, Electromagnetic induction by ocean currents and the electrical conductivity of the oceanic lithosphere: J. Geomagn. Geoelectr., **35**, 491–499.
Chave, A. D., and Filloux, J. H., 1984, Electromagnetic induction fields in the deep ocean off California: Oceanic and ionospheric sources: Geophys. J. Roy. Astr. Soc., **77**, 143–171.
———1985, Observation and interpretation of the seafloor vertical electric field in the eastern North Pacific: Geophys. Res. Lett., **12**, 793–796.
Chave, A. D., and Luther, D. S., 1990, Low frequency, motionally induced electromagnetic fields in the ocean 1., Theory: J. Geophys. Res., **95**, 7185–7200.
Chave, A. D., Filloux, J. H., Luther, D. S., Law, L. K., and White, A., 1989, Observations of motional electromagnetic fields during EMSLAB: J. Geophys. Res., **94**, 14153–14166.
Cheesman, S. J., Edwards, R. N., and Chave, A. D., 1987, On the theory of sea floor conductivity mapping using transient EM systems: Geophysics, **52**, 204–217.
Cheesman, S. J., Edwards, R. N., and Law, L. K., 1988, First results of a new short baseline sea floor transient EM system: Presented at the 58th Ann. Internat. Mtg., Soc. Explor. Geophys.
Coggon, J. H., and Morrison, H. F., 1970, Electromagnetic investigation of the seafloor: Geophysics, **35**, 476–489.
Constable, S. C., Parker, R. L., and Constable, C. G., 1987, Occam's inversion: a practical algorithm for generating smooth models from electromagnetic sounding data: Geophysics, **52**, 289–300.
Constable, S. C., Cox, C. S., and Chave, A. D., 1986, Offshore electromagnetic surveying techniques: 56th Ann. Internat. Mtg., Soc. Explor. Geophys.
Corliss, J. B., Dymond, J., Gordon, L. I., Edmond, J. M., von Herzen, R. P., Ballard, R. D., Green, K., Williams, D., Bainbridge, A., Crane, K., and van Andel, T. H., 1979, Submarine thermal springs on the Galapagos Rift: Science, **203**, 1073–1083.
Corwin, R. F., 1975, Offshore use of the self-potential method: Geophys. Prosp., **24**, 79–90.
———1983, Marine permafrost detection using galvanic electrical resistivity methods: Proc. Offshore Technology Conf., paper OTC 4480.
Corwin, R. F., Ebersole, W. C., and Wilde, P., 1970, A self-potential detection system for the marine environment: Proc. Offshore Technology Conf., paper OTC 1258.
Cox, C. S., 1980, Electromagnetic induction in the oceans and inferences on the constitution of the earth: Geophys. Surv., **4**, 137–156.
———1981, On the electrical conductivity of the oceanic lithosphere: Phys. Earth Plan. Int., **25**, 196–201.
Cox, C. S., Filloux, J. H., and Larsen, J. C., 1971, Electromagnetic studies of ocean currents and electrical conductivity below the ocean floor: *in* Maxwell, A. E., Ed., The Sea, Vol. 4, part 1: John Wiley, 637–693.
Cox, C. S., Kroll, N., Pistek, P., and Watson, K., 1978, Electromagnetic fluctuations induced by wind waves on the deep-sea floor: J. Geophys. Res., **83**, 431–442.
Cox, C. S., Filloux, J. H., Gough, D. I., Larsen, J. C., Poehls, K. A., Von Herzen, R. P., and Winter, R., 1980, Atlantic lithosphere sounding: J. Geomag. Geoelectr., **32**, suppl. I, SI13–SI32.
Cox, C. S., Constable, S. C., Chave, A. D., and Webb, S. C., 1986, Controlled-source electromagnetic sounding of the oceanic lithosphere: Nature, **320**, 52–54.
Degens, E. T., and Ross, D. A., Eds., 1969, Hot brines and recent heavy metal deposits in the Red Sea: Springer-Verlag.
Drysdale, C. V., 1924, The distribution of the magnetic field and return current around a submarine cable carrying alternating current—part I: Phil. Trans. Roy. Soc. **A224**, 95–140.
Duba, A., Heard, H. C., and Schock, R. N., 1974, Electrical conductivity of olivine at high pressure and under controlled oxygen fugacity: J. Geophys. Res., **79**, 1667–1673.
Edwards, R. N., 1988, Two-dimensional modeling of a towed in-line electric dipole-dipole sea-floor electromagnetic system: the optimum time delay or frequency for target resolution: Geophysics, **53**, 846–1853.
Edwards, R. N., and Chave, A. D., 1986, A transient electric dipole-dipole method for mapping the conductivity of the seafloor: Geophysics, **51**, 984–1987.
Edwards, R. N., and Cheesman, S. J., 1987, Two dimensional modelling of a towed transient magnetic dipole-dipole sea floor EM system: J. Geophys., **61**, 110–1121.
Edwards, R. N., Law, L. K., and DeLaurier, J. M., 1981, On measuring the electrical conductivity of the oceanic crust by a modified magnetometric resistivity method: J. Geophys. Res., **86**, 11609–11615.
Edwards, R. N., Nobes, D. C., and Gomez-Trevino, E., 1984, Offshore electrical exploration of sedimentary basins: the effects of anisotropy in horizontally isotropic, layered media: Geophysics, **49**, 566–576.
Edwards, R. N., Law, L. K., Wolfgram, P. A., Nobes, D. C., Bone, M. N., Trigg, D. F., and DeLaurier, J. M., 1985, First results of the MOSES experiment: Sea sediment conductivity and thickness determination, Bute Inlet, British Columbia, by magnetometric off-shore electrical sounding: Geophysics, **50**, 153–160.
Edwards, R. N., Wolfgram, P. A., and Judge, A. S., 1988, The ICE-MOSES experiment: Mapping permafrost zones electrically beneath the Beaufort Sea: Mar. Geophys. Res., in press.
Edwards, R. N., and Nabighian, M. N., 1991, Magnetometric resistivity method: *in* Nabighian, M. N., Ed., Electromagnetic methods in applied geophysics, Vol. 2, Soc. Expl. Geophys., This volume.
EMSLAB Group, 1988, The EMSLAB electromagnetic sounding experiment: EOS, **69**, 89, 98–99.

Filloux, J. H., 1967, An ocean bottom, D-component magnetometer: Geophysics, v. 32, p. 978–987.
———1973, Techniques and instrumentation for the study of natural electromagnetic induction at sea: Phys. Earth Plan. Int., **1**, 323–338.
———1974, Electric field recording on the sea floor with short span instruments: J. Geomag. Geoelectr., **26**, 269–279.
———1980a, Observation of very low frequency electromagnetic signals in the ocean: J. Geomag. Geoelectr., **32**, suppl. I, SII–SI12.
———1980b, Magnetotelluric soundings over the northeast Pacific may reveal spatial dependence of depth and conductance of the asthenosphere: E. Pl. Sci. Lett., **25**, 187–1195.
———1981, Magnetotelluric exploration of the North Pacific: Progress report and preliminary soundings near a spreading ridge: Phys. Earth Plan. Int., **25**, 187–195.
———1982, Magnetotelluric experiment over the ROSE area: J. Geophys. Res., **87**, 8364–8378.
———1987, Instrumentation and experimental methods for oceanic studies: *in* J. A. Jacobs, Ed., Geomagnetism, Vol. 1, London: Academic Press, 143–246.
Francis, T. J. G., 1977, Electrical prospecting on the continental shelf: Rep. Inst. Geol. Sci., 77/4, London: Her Majesty's Printing Office.
———1982, Large-scale resistivity experiment at Deep Sea Drilling Project Hole 459B: *in* Initial Reports of the Deep Sea Drilling Project, **60**, Washington, D.C.: US Government Printing Office, 841–852.
———1985a, Electrical methods in the exploration of seafloor mineral deposits: *in* Teleki, P. G., Dobson, M. R., Moore, J. R., and von Stackelberg, U., Eds., Marine Minerals, Dordrecht, Netherlands: D. Reidel, 413–420.
———1985b, Resistivity measurements of an ocean floor sulphide mineral deposit from the submersible Cyana: Mar. Geophys. Res., **7**, 419–438.
Hekinian, R., Franchetau, J., Renard, V., Ballard, R. D., Choukroune, P., Cheminee, J. L., Albarede, F., Minster, J. F., Charlou, J. L., Marty, J. C., and Boulegue, J., 1983, Intense hydrothermal activity at the axis of the East Pacific Rise near 13°N: Submersible witnesses the growth of sulfide chimney: Mar. Geophys. Res., **6**, 1–114.
Horne, R. A., and Frysinger, C. R., 1963, The effect of pressure on the electrical conductivity of seawater: J. Geophys. Res., **68**, 1967–1973.
Jupp, D. L. B., and Vozoff, K., 1975, Stable iterative methods for the inversion of geophysical data: Geophys. J. Roy. Astr. Soc., **42**, 957–976.
Kaufman, A. A., and Keller, G. V., 1981, The magnetotelluric sounding method: Elsevier.
———1983, Frequency and transient soundings: Elsevier.
Koski, R. A., Normark, W. R., and Morton, J. L., 1985, Massive sulfide deposits on the southern Juan de Fuca ridge: Results of investigations in the USGS study area, 1980–83: Mar. Min., **5**, 147–1164.
Lagabrielle, R., 1983, The effect of water on direct current resistivity measurement from the sea, river, or lake floor: Geoexpl., **21**, 165–170.
Larsen, J. C., 1968, Electric and magnetic fields induced by deep sea tides: Geophys. J. Roy. Astr. Soc., **16**, 47–70.
Law, L. K., and Greenhouse, J. P., 1981, Geomagnetic variation sounding of the asthenosphere beneath the Juan de Fuca Ridge: J. Geophys. Res., **86**, 967–978.
Lilley, F. E. M., Filloux, J. H., Bindoff, N. L., Ferguson, I. J., and Mulhearn, P. J., 1986, Barotropic flow of a warm-core ring from seafloor electric measurements: J. Geophys. Res., **91**, 12979–12984.
Luther, D. S., Chave, A. D., and Filloux, J. H., 1987, BEMPEX: a study of barotropic ocean currents and lithospheric electrical conductivity: EOS, **68**, 618–619, 628–629.
Nobes, D. C., Law, L. K., and Edwards, R. N., 1986, The determination of resistivity and porosity of the sediment and fractured basalt layers near the Juan de Fuca Ridge: Geophys. J. Roy. Astr. Soc., **86**, 289–1318.
Normark, W. R., Morton, J. L., Koski, R. A., and Clague, D. A., 1983, Active hydrothermal vents and sulfide deposits on the southern Juan de Fuca ridge: Geology, **11**, 158–163.
Oldenburg, D. W., 1983, Funnel functions in linear and nonlinear appraisal: J. Geophys. Res., **88**, 7387–7398.
Oldenburg, D. W., Whittal, K. P., and Parker, R. L., 1984, Inversion of ocean bottom magnetotelluric data revisited: J. Geophys. Res., **89**, 1829–1833.
Phillips, J. D., Driscoll, A. H., Peal, K. R., Marquet, W. M., and Owen, D. M., 1979, A new undersea geological survey tool: ANGUS: Deep. Sea Res., **26**, 211–1225.
Ranganayaki, R. P., and Madden, T. R., 1980, Generalized thin sheet analysis in magnetotellurics: an extension of Price's analysis: Geophys. J. Roy. Astr. Soc., 60, 445–457.
Rona, P. A., 1987, Ocean ridge crest processes: Rev. Geophys., **25**, 1089–1114.
Rona, P. A., Klinkhammer, G., Nelsen, T. A., Tretry, J. H., and Elderfield, H., 1986, Black smokers, massive sulfides, and vent biota at the Mid-Atlantic Ridge: Nature, **321**, 33–37.
Sato, M. and Mooney, H. M., 1960, The electrochemical mechanism of sulfide self-potentials: Geophysics, **25**, 226–249.
Schlumberger, C., Schlumberger, M., and Leonardon, E. G., 1934, Electrical exploration of water-covered areas: Trans. Am. Inst. Mining Metall. Eng., **110**, 122–134.
Segawa, J., Yukutake, T., Hamano, Y., Kasuga, T., and Utada, H., 1982, Sea floor measurement of geomagnetic field using newly developed ocean bottom magnetometers: J. Geomag. Geoelectr., **34**, 571–585.
Segawa, J., Hamano, Y., Yukutake, T., and Utada, H., 1983, A new model of ocean bottom magnetometer: J. Geomag. Geoelectr., **35**, 407–422.
Sorem, R. K., and Fewkes, R. H., 1979, Manganese Nodules: Plenum Press.
Spies, B., and Frischknecht, F. C., 1991, Electromagnetic sounding: *in* Nabighian, M. N., Ed., Electromagnetic methods in applied geophysics, Vol. 2, Soc. Expl. Geophys., this volume.
Spiess, F. N., MacDonald, K. C., Atwater, T., Ballard, R., Carranza, A., Cordoba, D., Cox, C., Diaz Garcia, V. M., Francheteau, J., Guerrero, J., Hawkins, J., Haymon, R., Hessler, R., Juteau, T., Kastner, M., Larson, R., Luyendyk, B., MacDougall, J. D., Miller, S., Normark, W., Orcutt, J., and Rangin, C., 1980, East Pacific Rise: hot springs and geophysical experiments: Science, **207**, 1421–1433.
Tarits, P., 1986, Conductivity and fluids in the oceanic upper mantle: Phys. E. Pl. Int., **42**, 215–226.
Teleki, P. G., Dobson, M. R., Moore, J. R., and von Stackelberg, U., (eds.), 1985, Marine Minerals, Dordrecht, Netherlands: D. Reidel.
Von Herzen, R. P., Francis, T. J. G., and Becker, K., 1983, In situ large-scale electrical resistivity of ocean crust, Hole 504B: *in* Cann, J. R., Langseth, M. G., Honnorez, J., von Herzen, R. P., White, S. M., Eds., Initial Reports of the Deep Sea Drilling Project, **69**, Washington D.C.: US Government Printing Office.
Vozoff, K., 1972, The magnetotelluric method in the exploration of sedimentary basins: Geophysics, **37**, 98–141.
Vozoff, K., 1991, The magnetotelluric method: *in* Nabighian, M. N., Ed., Electromagnetic methods in applied geophysics, Vol. 2, Soc. Expl. Geophys., this volume.
Ward, S. H. and Hohmann, G., 1988, Electromagnetic theory for geophysical applications: *in* Nabighian, M. N., Ed., Electromagnetic Methods in Applied Geophysics, vol. 1: Soc. Expl. Geophys., 131–311.
Webb, S. and Cox, C. S., 1982, Electromagnetic fields

induced at the seafloor by Rayleigh-Stoneley waves: J. Geophys. Res., **87**, 4093–4102.
Webb, S. and Cox, C. S., 1986, Observations and modeling of seafloor microseisms: J. Geophys. Res., **91**, 7343–7358.
Webb, S., Constable, S. C., Cox, C. S., and Deaton, T. K., 1985, A seafloor electric field instrument: J. Geomagn. Geoelectr., **37**, 1115–1129.
White, A., 1979, A sea floor magnetometer for the continental shelf: Mar. Geophys. Res., **4**, 105–114.
Wolfgram, P. A., Edwards, R. N., Law, L. K., and Bone, M. N., 1986, Polymetallic sulfide exploration on the deep sea floor: The feasibility of the MINI-MOSES technique: Geophysics, **51**, 1808–1818.
Wynn, J. C., 1988, Titanium geophysics: the application of induced polarization to seafloor mineral exploration: Geophysics, **53**, 386–401.
Young, P. D. and Cox, C. S., 1981, Electromagnetic active source sounding near the East Pacific Rise: Geophys. Res. Lett., **8**, 1043–1046.

APPENDIX: ELECTROMAGNETIC INDUCTION EQUATIONS

The approach taken here closely follows the treatment of Chave and Luther (1990). The Maxwell equations in the quasi-static limit with all electric current terms except the conduction current neglected are

$$\nabla \cdot \mathbf{B} = 0 \tag{A-1}$$

$$\nabla \times \mathbf{E} + \partial_t \mathbf{B} = 0 \tag{A-2}$$

$$\nabla \times \mathbf{B} - \mu_0 \sigma \mathbf{E} = \mu_0 \mathbf{J} \tag{A-3}$$

where $\mathbf{E}$ and $\mathbf{B}$ are the electric field and magnetic induction, μ_0 is the magnetic permeability of free space, σ is the electrical conductivity, and $\mathbf{J}$ is the impressed source electric current density. Using a Mie representation (Backus, 1986), the magnetic induction may be written

$$\mathbf{B} = \hat{\mathbf{z}} \times \nabla_h \Pi + \nabla_h \partial_z \Psi - \nabla_h^2 \Psi \hat{\mathbf{z}} \tag{A-4}$$

where ∇_h denotes the horizontal gradient operator and Π and Ψ are scalar functions representing toroidal and poloidal magnetic (TM and PM) modes, as discussed in the text. The source current in equation (A-3) may be decomposed in a similar way to equation (A-4)

$$\mathbf{J} = \hat{\mathbf{z}} \times \nabla_h Y + \nabla_h T + \Xi \hat{\mathbf{z}} \tag{A-5}$$

where Ξ is the vertical part of the source current and Y and T are scalar functions which satisfy the Poisson equations

$$\nabla_h^2 Y = (\nabla \times \mathbf{J}) \cdot \hat{\mathbf{z}} \tag{A-6}$$

$$\nabla_h^2 T = \nabla_h \cdot \mathbf{J}. \tag{A-7}$$

If the electric field is also written in terms of three scalars, the conductivity profile is assumed to vary only vertically, and the Cartesian components of equations (A-2) and (A-3) are written out explicitly, it can be shown, using the properties of analytic functions of a complex variable, that the modal scalars satisfy the differential equations

$$\nabla_h^2 \Pi + \sigma \partial_z (\partial_z \Pi / \sigma) - \mu_0 \sigma \partial_t \Pi = \mu_0 \Xi - \mu_0 \sigma \partial_z (T/\sigma) \tag{A-8}$$

$$\nabla^2 \Psi - \mu_0 \sigma \partial_t \Psi = \mu_0 Y \tag{A-9}$$

and the electric field is given by

$$\mathbf{E} = \hat{\mathbf{z}} \times \nabla_h \partial_t \Psi - \nabla_h [(\partial_z \Pi / \mu_0 + T)/\sigma] + (\nabla_h^2 \Pi / \mu_0 - \Xi)/\sigma \hat{\mathbf{z}}. \tag{A-10}$$

The differences between equation (A-8) and equation (A-9) are caused by the nature of the electric currents associated with the two modes. Equation (A-8) reduces to that for dc resistivity sounding in the zero frequency limit, while equation (A-9) is the usual diffusion equation of EM induction.

The modal equations can be solved conveniently by constructing Green functions which incorporate the necessary EM boundary conditions at the seafloor and sea surface, which are assumed to be flat interfaces. Assuming $e^{i\omega t}$ time dependence, expressing the horizontal spatial components as the Fourier transform pair defined by

$$\hat{\mathbf{f}}(\eta, \xi) = \int\int_{-\infty}^{\infty} dx\, dy\, f(x, y) e^{i(\eta x + \xi y)}$$

and

$$f(x, y) = \frac{1}{(2\pi)^2} \int\int_{-\infty}^{\infty} d\eta\, d\xi\, \hat{\mathbf{f}}(\eta, \xi) e^{-i(\eta x + \xi y)} \tag{A-11}$$

and assuming an ocean depth H and conductivity σ_0, then placing the coordinate origin ($z = 0$) at the seafloor yields

$$\hat{\Pi} = \mu_0 \int_0^H dz'\, g_\pi(z, z')\hat{\Xi}(z') + \mu_0 \int_0^H dz'\, \partial_{z'} g_\pi(z, z')\hat{\mathbf{T}}(z') \quad \text{(A-12)}$$

$$\hat{\Psi} = \mu_0 \int_0^H dz'\, g_\psi(z, z')\hat{\mathbf{Y}}(z, z') \quad \text{(A-13)}$$

where the Green functions are

$$g_\pi(z, z') = -[e^{-\beta|z - z'|} + R_L^{\mathrm{TM}} e^{-\beta(z + z')} - e^{-2\beta H} e^{\beta(z + z')} - R_L^{\mathrm{TM}} e^{-2\beta H} e^{\beta|z - z'|}]/ \times [2\beta(1 + R_L^{\mathrm{TM}} e^{-2\beta H})] \quad \text{(A-14)}$$

$$g_\psi(z, z') = -[e^{-\beta|z - z'|} + R_L^{\mathrm{PM}} e^{-\beta(z + z')} + R_A^{\mathrm{PM}} e^{-2\beta H} e^{\beta(z + z')} + R_A^{\mathrm{PM}} R_L^{\mathrm{PM}} e^{-2\beta H} e^{\beta|z - z'|}]/ \times [2\beta(1 - R_A^{\mathrm{PM}} R_L^{\mathrm{PM}} e^{-2\beta H})]. \quad \text{(A-15)}$$

The reflection coefficients at the seafloor and sea surface in equations (A-14) and (A-15) are

$$R_L^{\mathrm{TM}} = (\beta K/\sigma_0 - 1)/(\beta K/\sigma_0 + 1)$$

$$R_A^{\mathrm{PM}} = (\beta - k)/(\beta + k)$$

$$R_L^{\mathrm{PM}} = (\beta\Lambda - 1)/(\beta\Lambda + 1) \quad \text{(A-16)}$$

where K and Λ are TM and PM mode response functions which contain all of the information on conductivity below the seafloor necessary to solve the problem and the induction parameter is

$$\beta = \sqrt{k^2 + i\omega\mu_0\sigma_0} \quad \text{(A-17)}$$

with the composite wavenumber given by $k = (\eta^2 + \xi^2)^{1/2}$. Expressions for the modal response functions for both layered and continuous conductivity profiles are given in Chave and Cox (1982), and their different functional forms are caused by the disparate sensitivity of the two modes to electrical structure. Since the reflection coefficients are in general complex, the EM induction phenomena they represent are complicated, involving leaky surface or evanescent waves.

The EM fields produced by any controlled source type follow by integrating equations (A-12) and (A-13) over the vertical dimensions of the source, inverting to the spatial domain using equation (A-11), and completing the source integration. The EM fields are then computed using equations (A-4) and (A-10). The Fourier transform may be converted to a Hankel transform for sources of simple symmetry using the usual procedure of converting equation (A-11) to polar coordinates. Because of the complexity of equations (A-14) and (A-15), evaluation of these closed-form expressions must be done numerically.